STRUCTURAL INSIGHTS INTO PLANT CELL PROLIFERATION DISTURBANCE BY AGROBACTERIUM PROTEIN 6B

WANG MEIMEI

NATIONAL UNIVERSITY OF SINGAPORE

2010

STRUCTURAL INSIGHTS INTO PLANT CELL PROLIFERATION DISTURBANCE BY AGROBACTERIUM PROTEIN 6B

WANG MEIMEI

A THEIS SUBMITTED

FOR THE DEGREE OF MASTER OF BIOLOGY

DEPARTMENT OF BIOLOGICAL SCIENCES

NATIONAL UNIVERSITY OF SINGAPORE

2010

Acknowledgements

I would like to express my sincere gratitude to my dear supervisor Assistant Professor Yuan Yu-Ren, Adam for his guidance, encouragement and help. I also want to express my utmost respect to him as a dedicated scientist.

I thank Dr. HongYan for allowing me to do Real-time RT-PCR in his lab. Thank Ms Mao Huizhu for allowing me to do transgenic plant selection in her tissue culture room. Thank Dr. Chengxiang and Dr. Zhaojing for showing me how to do particle bombardment. I also thank Dr. Graham and Ms Fiona for teaching and helping me to use the fluorescence microcope.

I am grateful to Dr. HongYing, Ye Jian, Qu jing, Ge Yunfeng in Prof. Chua's lab and Dr. Ailing in Dr. HongYan's lab for their invaluable suggestions and help in my project.

I would also acknowledge the financial support of Singapore Ministry of Education. Thank Temasek Life Science Laboratory for providing facilities. Lastly, I am also grateful to all the people in our lab for their assistance and anyone who have helped me throughout the course of my study in one way or another. Especially thank my friend and workmate, Dr. Yang Xia for her friendship, encouragement and emotional support.

Table of Content

ACKNOWLEDGEMENTS I

TABLE OF CONTENT II

SUMMARY IV

LIST OF FIGURES V

LIST OF TABLES V

CHAPTER 1 INTRODUCTION 1

1.1 RESEARCH PROGRESS ON *6B* GENES 1
1.2 OBJECTIVES OF THIS RESEARCH AND POTENTIAL CONTRIBUTION 4

CHAPTER 2 GENERAL MATERIALS AND METHODS 5

2.1 MEDIA AND BUFFER 5
2.1.1 Media 5
2.1.2 Buffer 5
2.2 PLASMIDS AND COMPETENT *ESCHERICHIA COLI* STRAINS CELLS 5
2.3 PLANT MATERIALS 7
2.4 MOLECULAR CLONING 7
2.4.1 Polymerase chain reaction (PCR) 7
2.4.2 Construction of Plasmids 8
2.4.3 Purification of PCR fragments and isolation of DNA fragments from agarose gel 12
2.4.4 Ligation of DNA inserts into plasmid vectors 12
2.4.5 Transformation of bacteria with ligation mixture or plasmid 12
2.4.6 Purification of plasmids from bacteria in a small scale 13
2.4.7 Screening of transformants by restriction digestion and DNA sequencing 13
2.5 *AGROBACTERIUM* TRANSFORMATION OF *ARABIDOPSIS* 14
2.6 NUCLEI ACID ISOLATION AND REVERSE TRANSCRIPTION (RT)-PCR 15
2.7 PROTEIN EXPRESSION AND PURIFICATION 16
2.7.1 Induction of protein expression in bacteria 16
2.7.2 Protein purification 17
2.7.3 Sodium dodecylsulfate-polyacrylamide electrophoresis (SDS-PAGE) 18
2.8 PROTEIN CRYSTALLIZATION 19
2.8.1 Light scattering 19
2.8.2 Hanging drop crystallization 19
2.9 DATA COLLECTION 20
2.10 STRUCTURE DETERMINATION 21
2.11 *IN VITRO* PULL-DOWN ASSAYS 22

2.12 Co-immunoprecipitation experiments 22
2.13 Western blot analyses 23
2.14 Northern blot analysis 23
2.15 Real-time RT-PCR 24
2.16 Transient Expression of Fluorescent Protein Fusions in Onion Cells 26

CHAPTER 3 RESULTS 28

3.1 Expression and purification of 6b proteins 28
3.2 Overall Crystal structures of AK6b and AB6b 35
3.3 6b shares structural similarities with ADP-ribosylating toxins 36
3.4 Putative NAD^+ binding site of 6b 38
3.5 Target binding loop 42
3.6 6b interferes with miRNAs pathways in *Arabidopsis* 46
3.7 6b targeting Arabidopsis AGO1 and SE *in vitro* and *in vivo* 51

CHAPTER 4 DISCUSSION 58

4.1 6b belongs to a novel toxin family 58
4.2 6b directly targets miRNA machineries 60
4.3 Potential roles of 6b on plant gene regulation and cell growth 64

REFERENCES 67

APPENDIX 73

PUBLICATIONS 81

Summary

The *Agrobacterium* T-DNA *6b* protein has weak sequence similarity to other *RolB* family proteins, which can cause callus formation on tobacco leaf discs without the presence of auxin. 6b proteins interact with many different proteins involved in expression of plant genes related to cell proliferation. Here, we report the crystal structures of *Agrobacterium tumefaciens* AK6b at 2.1 Å and *Agrobacterium vitis* AB6b at 1.65 Å. The 6b structure adopts an ADP-ribosylating toxin fold and represents a new toxin family with Tyr66, Thr93 and Tyr153 as the putative ADP-ribosylation catalytic residues. We showed that overexpression of 6b in *Arabidopsis* displays miRNA deficiency phenotype and a specific loop fragment (residues 40-55) of 6b is needed for specific direct binding to SERRATE and AGO1. Our work provides structural insights suggesting that 6b affects the growth of plant cells probably via its ADP-ribosylation activity and the disturbance of miRNA pathway.

List of Figures

FIG. 1 SEQUENCE ALIGNMENT OF 6B GENES WITH ROLB. 28
FIG. 2 EXPRESSION AND PURIFICATION OF AK6B PROTEIN. 29
FIG. 3 EXPRESSION AND PURIFICATION OF NHIS-AB6B PROTEIN. 30
FIG. 4 15% SDS-PAGE OF PURIFIED AK6B AND AB6B USED FOR CRYSTALLIZATION. 30
FIG. 5 IMAGE OF AK6B CRYSTALS (40X MAGNIFICATION). 32
FIG. 6 DIFFRACTION PATTERN FROM A WELL-FORMED AK6B CRYSTAL. 32
FIG. 7 IMAGE OF AB6B CRYSTALS (40X MAGNIFICATION). 33
FIG. 8 DIFFRACTION PATTERN FROM A WELL-FORMED AB6B CRYSTAL. 33
FIG. 9 OVERALL STRUCTURE OF *AGROBACTERIUM* PROTEIN 6B. 36
FIG. 10 AK6B IS AN ADP-RIBOSYLATING TOXIN. 39
FIG. 11 EFFECTS OF TAD ON MORPHOLOGY OF *35S::AK6B* TRANSGENIC *ARABIDOPSIS*. 40
FIG. 12 PUTATIVE ACTIVE SITE OF AK6B. 41
FIG. 13 PROTEIN-PROTEIN INTERACTION LOOP OF AK6B. 46
FIG. 14 EXPRESSION OF MIRNA IN *AK6B* TRANSGENIC PLANTS. 49
FIG. 15 NORTHERN BLOT RESULTS SHOWED THE ACCUMULATION OF SMALL RNAS IN WT (*COL-0*), *SE-1* AND *35S::AK6B* PLANTS. 50
FIG. 16 REAL-TIME RT-PCR RESULTS SHOWED THE ACCUMULATION OF THE TARGET MRNAS IN WT (*COL-0*), *SE-1* AND *35S::AK6B* PLANTS. 50
FIG. 17 INTERACTION OF AK6B AND AGO1 *IN VITRO* AND *IN VIVO*. 52
FIG. 18 INTERACTION OF AK6B AND SE *IN VITRO* AND *IN VIVO*. 53
FIG. 19 *IN VITRO* PULL DOWN ASSAYS OF 6B PROTEINS WITH HIS-SE CORE FRAGMENT. 54
FIG. 20 INTERACTION OF AK6B AND SE FRAGMENTS IN *ARABIDOPSIS* PLANTS *IN VIVO*. 55
FIG. 21 PLASMIDS USED FOR BOMBARDMENT INTO ONION EPIDERMAL CELLS. 57
FIG. 22 AK6B COLOCALIZES WITH AGO1 OR SE IN THE NUCLEUS. 57
FIG. 23 A HYPOTHETICAL WORKING MODEL DESCRIBING THE ROLES OF 6B ON PLANT GENE REGULATION. 66

List of Tables

Table 1: Data collection, phasing and refinement statistic…….. 34

Chapter 1 Introduction

The gram-negative soil bacterium *Agrobacterium* is a phytopathogen by virtue of its ability to transform normal plant cells into tumor cells. This eventually results in tumor formation at wound sites of infected dicotyledonous plants. During tumor induction *Agrobacterium* attaches to plant cells and then transfers part of its tumor-inducing (Ti) plasmid to some of these plant cells. The transferred T-DNA region (the segment of DNA that is surrounded by 24 basepair imperfect direct repeats or border repeats in the Ti plasmid) becomes integrated into one of the chromosomes of the plant cell. Expression of the genes located on the T-DNA region leads to the formation of proteins involved in the production of indole acetic acid (an auxin) and isopentenyl-AMP (a cytokin). These plant hormones cause the tumorous phenotype that is characterized by the ability of the plant cells to proliferate limitlessly and autonomously even in the absence of added phytohormones. Crown gall tumors are characterized by the production of opines is catalysed by opine synthases, which are encoded by the T-DNA.

1.1 Research progress on *6b* genes

The molecular mechanism underlying such a kind of bacterium-plant interaction has been described in some detail. Many *Agrobacterium* T-DNA genes belong to the family of so-called developmental plasticity (*plast*) genes (Levesque et al., 1988). This family includes genes *3'*, *5*, *6a*, *6b*, *rolB*, *rolC*, *orf8*, *orf13*, *lso*, and various other T-DNA genes. Amongst the plast genes, a gene designated as *6b*, which is localized at

the *tml* locus (Garfinkel et al., 1981), has been found in all T-DNA of all strains of *Agrobacterium* (Willmitzer et al., 1983). *6b* appears to play a role in the expression of plant genes related to cell proliferation and the modification of the morphology of crown galls, although the *6b* gene itself is not required for the formation of the latter (Garfinke et al., 1981; Tinland et al., 1992).

The *6b* genes have remarkable and unique effects on plant growth. They induce tumors on stems in a limited number of plant species, including *Nicotiana glauca* (Hooykaas et al., 1988; Tinland et al., 1989; Kitakura et al., 2002), grapevine (Huss et al., 1990) and *N. rustica* (Garfinke et al., 1981; Paulus et al., 1991); increase wound-induced division of cells in *N. rusica* (Tinland et al., 1992); promote *iaa*- and *ipt*-induced cell division (Tinland et al., 1989; Hooykaas et al., 1988); enhance tumor formation or increase the size of crown galls induced on *N.rustica* by the action of the *auxin* genes and the *cytokinin* gene (Tinland et al., 1989). Expression of *6b* genes also elicit morphological and anatomical changes in tobacco plants, modify cotyledons, flowers, petioles, stems and roots (Tinland et al., 1990; Tinland et al., 1992; Helfer et al., 2003; Gremillon et al., 2004); develop enations, catacorollas, tubular leaves, fragmented leaf primordia, hyponastic petioles and epinastic leaf veins (Clément et al., 2006).

The predicted amino acid sequence of *6b* is distantly-related to the RolB family proteins, whose expression also result in aberrant growth and abnormal morphology of both roots and shoots (Spena et al., 1987; Stieger et al., 2004; Levesque et al., 1988). Protein 6b localizes to the nucleus and was reported to bind to many nuclear

proteins, such as NtSIP1 (Nicotiana tabacum Six-b Interacting Protein 1, Kitakura et al., 2002), NtSIP2 (Nicotiana tabacum Six-b Interacting Protein 2, Kitakura et al., 2008) and histone H3 (Terakura et al., 2007) and affects the expression of various plant genes in transgenic *Arabidopsis*. Transgenic *Arabidopsis* plants expressing the *AK6b* gene display leaf abnormality at early developmental stages, such as leaf upward curling and serration, protrusion on the abaxial side of the leaf, altered flower structure and callus formation on hormone-free medium. Notably, the morphology phenotypes of *AK6b* transgenic plants partially overlap with those of miRNA-deficient mutant lines, such as *ago1-27* and *se-1*.

Much effort has been made to elucidate the 6b function at both the cellular and molecular levels. So far, different hypotheses have been proposed to explain the effects of *6b* on the growth of plant cells. *6b* gene could possess auxin- and cytokinin-like activity by modulating auxin or cytokinin receptors and promote activity of genes involved in auxin and cytokinin biosynthesis (Wabiko and Minemura, 1996; Clément et al., 2006). *6b* might induce plants to synthesize a phloem-mobile growth factor (enation factor) (Helfer et al., 2003). In addition, *6b* gene is also proposed to modulate the metabolism of phenolic compounds (Galis et al., 2002; Galis et al., 2004; Kakiuchi et al., 2006), induce changes in gene expression resulting in phenylpropanoid changes (Kitakura et al., 2002; Terakura et al., 2006), modify osmotic controls required for normal and wound-induced cell expansion (Clément et al., 2006) and cause the absorption, retention and abnormal accumulation of sugars (Clément et al., 2007).

Recent studies on *6b* further suggest that *6b* might affect chromatin status as a

chromatin chaperon or affect the expression of class I KNOX, CUC, IAA and cell cycle-related genes as a transcriptional regulator of proliferation of plant cells in tobacco and *Arabidopsis* (Terakura et al., 2006; Terakura et al., 2007).

1.2 Objectives of this research and Potential contribution

Although, much work has been done on 6b, the exact functional role of 6b at the molecular level remains unknown due to the lack of structural motif information obtained from 6b sequences. As a first step to investigate the molecular mechanism of leaf abnormality introduced by 6b overexpression in plants, we now report on the high-resolution crystal structures of AK6b and AB6b. Our data demonstrate that 6b displays a novel ADP-ribotransferase fold quite close to that of cholera toxin. However it has a completely different set of catalytic residues within the substrate-binding pocket, although the overall fold of 6b is quite close to that of Cholera toxin. We further discovered that 6b disturbs miRNA pathway by targeting miRNA processing machinery and slicing machinery.

Chapter 2 General Materials and Methods

2.1 Media and Buffer

2.1.1 Media

LB liquid medium: 1% Bacto®- tryptone, 0.5% Bacto®- yeast extract, 0.5% NaCl, pH 7.5, autoclaved at 121°C for 20 min and cooled at room temperature.

LB agar: LB medium with 1.5% Bacto®- agars, pH 7.5. The medium mixed with plasmids related antibiotics was transferred to sterile Petri dishes after cooling down.

2×YT liquid medium: 16g Bacto Typtone, 10g Bacto Yeast extract and 5g NaCl. Adjust pH to 7.0 with 5N NaCl. Fill up to 1L with ddH2O. Sterilize by autoclaving for 20min.

Murashige and Skoog medium (MS): see Table A1.

2.1.2 Buffer

50×TAE: 2M Tris base，0.57M Acetic acid glacial，50M EDTA，pH 8.3.

TBE: 89 mM Tris-borate, 2 mM EDTA, pH 8.3.

TE: 10 mM Tris-HCl, 1 mM EDTA, pH 8.0.

PBS (Phosphate buffered saline): 140mM NaCl, 2.7mM KCl, 10mM Na_2HPO_4, 1.8mM KH_2PO_4, pH 7.3.

2.2 Plasmids and competent *Escherichia coli* strains cells

The vectors pET-28b (Figure A1), pGEX-6P-1 (Figure A2), and pMAL-c2X

(Figure A3) were used for protein expression in bacterial *E.coli* system. The pBI121 vector (Figure A4) was used for *Arabidopsis* Floral dipping. The pBA002-YFP and pBA002-CFP (Figure A5) were used for colocalization in onion epidermal cells. The bacterial strains used were *Escherichia coli* BL21 (DE3), DH5α, XL1- blue and EHA105.

Competent cells of BL21 (DE3), DH5α and XL1-Blue were prepared with calcium chloride ($CaCl_2$) method (Sambrook *et al*., 1989). Briefly, a single colony from freshly streaked LB plate were inoculated into 2ml LB medium and incubated overnight at 37°C with vigorous shaking before transferring to 100 ml LB medium, then continue growing to an OD_{600} of 0.4 to 0.6 at 37°C with vigorous shaking. Culture was transferred to falcon tubes and kept in ice for 10 min, was centrifuged at 4000 rpm for 10 min at 4°C. The pellet was re-suspended in 10 ml of ice-cold 0.1M $CaCl_2$ and incubated in an ice bath for 30 min. Then the centrifuge step was repeated once. 2 ml ice-cold $CaCl_2$ was added to re-suspend the cell pellet, gently mixed with autoclaved glycerol to a final concentration of 20%. Then 100µl of the cells was aliquoted to each tube and were kept at -80°C.

The competent cell of EHA105 was prepared especially for electroporation. Preferably, select single colony from fresh LB plate for inoculating a 10ml 2×YT overnight starter culture in 37^{o}C shaker (250rpm). Inoculate 1L of 2×YT media, grow cells at 37^{o}C and then remove the cells to ice box when OD_{600} equals 0.6-0.9. Collect the pellet by spinning at 4000rpm for 25min at 4^{o}C. Gently resuspend the pellet in 800ml ice-cold ddH_2O. Repeat the washing step again. And then gently

resuspend the pellet in 4ml of ice-cold 10% glycerol. Final OD_{600} of resuspended cells equals 200-250. Then 100µl of the cells was aliquoted to each tube and were kept at -80°C.

2.3 Plant materials

For TAD (thiazole-4-carboxamide adenine dinnucleotide) inhibition assay, northern blot and real-time RT-PCR, *se-1*, *ago1-27* mutant and all *6b* transgenic plants used are in the *Col-0* background. Seeds including the wild type *Arabidopsis thaliana* (*Col-0*) were surface sterilized and germinated on MS medium with 1% agar containing Gamborg's Vitamin Solution (Sigma). After 2 days of vernalization at 4^{o}C, seeds were incubated at 22^{o}C under long day light condition.

Fresh onion bulbs used for particle bombardment were purchased from local grocery store.

2.4 Molecular cloning

2.4.1 Polymerase chain reaction (PCR)

PCR reaction was set up for 50 µl of volume in a 0.5 ml microfuge PCR tube as bellow: 1×Tag PCR buffer, 0.2 mM of each dNTP, 1 mM $MgCl_2$, 1 µM of each primer, 1 units of polymerase and 10 ng/µl of DNA template. Amplification was performed in Applied Biosystems GeneAmp PCR System 9700 using specific program according to different reactions. PCR products were then examined by 1% agarose gel electrophoresis.

2.4.2 Construction of Plasmids

Plasmids and their relevant characteristics are listed in Table A2. All manipulations for construction of plasmids were performed using standard techniques (Sambrook et al., 1989). All the constructs were verified by sequencing. *Escherichia coli* DH5α or XL1- blue was used as host for plasmids construction.

A series of 6b related vectors were constructed as follows. Full-length *AK6b* from pTiAKE10 and *AB6b* from pTiAB4 were cloned using the same specific primers:

F: 5'-ATGACGGTTCCTACTTGG-3'

R: 5'-CTAACGTGTGAGATGGCAC-3'

Mutants of *AK6b* were prepared by overlapping PCR. The primers for overlapping PCR are listed in Table A3. The PCR fragments for protein synthesis in *E. coli* with His-tag or GST-tag or MBP-tag were digested with *NdeI/XhoI* or *EcoRI/XhoI* or *EcoRI/HindIII*. The primers are as following:

NdeI-N: 5'-GATGCAcatATGACGGTTCCTACTTGGC-3'

XhoI-n: 5'-GTAGCTctcgagTTACTAACGTGTGAGATGGCAC-3'

EcoRI-GST: 5'-GATGCAgaattcATGACGGTTCCTACTTGGC-3'

XhoI-gst: 5'-GTAGCTctcgagTTACTAACGTGTGAGATGGCAC-3'

EcoRI-MBP: 5'-GATGCAgaattcATGACGGTTCCTACTTGGC-3'

HindIII-mbp: 5'-GTAGCTaagcttTTACTAACGTGTGAGATGGCAC-3'

The resulting fragments were ligated into pET-28b (kanamycin selection, Novagen), pGEX-6p-1 (ampicillin selection, Novagen), or pMAL-c2X (ampicillin selection, Novagen) vectors, respectively, to yield pET-AK6b, -AB6b; pGEX- AK6b, -AB6b, -200; pMAL-40, -164. The PCR fragments for transformation of A*rabidopsis* were

digested with *XbaI/SacI*. The primers are:

XbaI-35S: 5'- GATGCAtctagaATGACGGTTCCTACTTGG-3'

SacI-35s: 5'- GTAGCTgagctcCTAACGTGTGAGATGGCAC-3'

The resulting fragments were linked to the cauliflower mosaic virus 35S promoter in the binary vector pBI121 to yield *p121-AK6b*, *-40*, *-66*, *-93*, *-116*, *-121*, *-123*, and *-146*.

For the construction of colocalization of 6b with Ago1 or SE, the AK6b, AGO1 or SE full-length cDNA was amplified from a clone in related plasmid by PCR using the following primers:

AK6b:

F: 5'-GATGCActcgagATGACGGTTCCTACTTGGC-3'

R: 5'-GATGCAacgcgtACGTGTGAGATGGCACGAT-3'

AGO1:

F: 5'-GATGCActcgagATGGTGAGAAAGAGAAGAACG-3'

R: 5'-GATGCAacgcgtGCAGTAGAACATGACACGCT-3'

SE:

F: 5'-GATGCActcgagATGGCCGATGTTAATCTTC-3'

R: 5'-GATGCAacgcgtCAAGCTCCTGTAATCAATAAC-3'

The forword primers adds an *XhoI* site (underlined) to the 5'-end of the PCR product, while the reverse primer omits the stop codon of the target genes cDNA and adds an *MluI* site (underlined) to the 3'-end of the amplified DNA. The resulting *AK6b* cDNA fragment was cloned into the pBA002-CFP (cyan fluorescent protein) (spectinomycin

selection, Novagen) plasmid so that the 3'-end of AK6b coding sequence was fused to the 5'-end of CFP in frame, and the whole gene lied downstream of and was under the control of the cauliflower mosaic virus (CaMV) 35S promoter. For the AGO1 and SE cDNA, the target plasmid was pBA002-YFP (yellow fluorescent protein) (spectinomycin selection, Novagen). The cloning procedure was same. The sequence of the chimeric *AK6b-CFP*, *SE-YFP* or *AGO1-YFP* gene in the pBA002 plasmid was checked by DNA sequencing and was found to be correct and in-frame.

Histone *H3* was cloned from *Col-0* genomic DNA using the following primers with a *BamHI* site (underlined) at the forword primer H3F and an *XhoI* site (underlined) at the reverse primer H3R.

H3F: 5'-GATGCAggatccATGGCTCGTACCAAGCAA -3'

H3R: 5'-GTAGCTctcgagTCATTAAGCACGTTCTCCAC-3'

PCR product was digested then with *BamHI/XhoI* and inserted into pET-28b-SUMO vector (kanamycin selection, Novagen), which is similar to pET-28b with a sumo-tag fusioned just followed to his-tag to yield His-SUMO-H3.

Truncated forms of *AGO1* cDNA were cloned using following sets of primers with related digestion sites (underlined):

PolyQ (1-187aa of AGO1):

F: 5'- GATGCAtctagaATGGTGAGAAAGAGAAGAACG -3'

R: 5'- GTAGCTaagcttTTACTGTCCTTTACCAGGCCTC -3'

NT (185-371aa of AGO1):

F: 5'- GATGCAtctagaATGAAAGGACAGAGTGGAAAGC -3'

R: 5’- GTAGCTaagcttTTAGCCCATCTGTGTAGGACG -3’

PAZ (366-566aa of AGO1):

F: 5’- GATGCAtctagaATGCGTCCTACACAGATGGGC -3’

R: 5’- GTAGCTaagcttTTACTGTCCTTTACCAGGCCTC -3’

MID (559-675aa of AGO1):

F: 5’–GATGCAgaattcATGGCTTCTGTTGAGGCTCGTA -3’

R: 5’- GTAGCTaagcttTTAATCAATTTCTTTTCCTTGGG-3’

PIWI1 (674-836aa of AGO1):

F: 5’- GATGCAgaattcATGATTGATCTGCTTATTGTCATTCT -3’

R: 5’- GTAGCTaagcttTTAATGCCCAGTTGATCTACGG -3’

PIWI2 (829-1049aa of AGO1):

F: 5’- GATGCAgaattcATGGCCTTCCGTAGATCAACTG -3’

R: 5’-GTAGCTaagcttTTATCAGCAGTAGAACATGACACG-3’

The PCR fragments were digested with *XbaI/HindIII* for NT, L1 and PAZ, and *EcoRI/HindIII* for Mid, PIWI1 and PIWI2. The resulting fragments were ligated into the pMAL-c2X vector backbone to yield pMAL- PolyQ, - NT, - PAZ, - MID, - PIWI1 and - PIWI2.

cDNA encoding SE core (residues 194-543) was cloned in frame into pET-28b vector with a C-terminal 6×His-tag, yield pET-SE. N terminal (residues 194-240) and middle domain (residues 248-470) of SE was cloned into pGEX-6p-1 vector, respectively, to yield pGEX-Mid or pGEX-NT.

2.4.3 Purification of PCR fragments and isolation of DNA fragments from agarose gel

The amplified PCR product was separated in 1% agarose gel. When only one specific band was obtained from the reaction, the PCR product was purified directly by using the QIAGEN PCR Purification System; when there were unspecific bands, the desired band was excised from the gel under long wavelength UV light and the DNA was purified using the QIAGEN Gel Extraction Kit according to the manufacturer's instructions.

2.4.4 Ligation of DNA inserts into plasmid vectors

After the plasmid vectors and DNA fragments were digested with suitable restriction enzymes and purified, ligation reaction was set up to 10 µl of volume in a 0.2 ml microfuge tube as bellow: 1 × reaction buffer, molar ratio of DNA insert to vector is 3:1, 2 units of T4 DNA ligase (Rapid DNA ligation kit, Roche, Germany). The reaction was incubated at room temperature for 10min.

2.4.5 Transformation of bacteria with ligation mixture or plasmid

Competent cells were thawed on ice and 10µl ligation mixture or 1µl of the plasmid was added to the 50ul competent cells and mixed gently. For heat shock transformation, after incubation on ice for 20 min, the mixture was subjected to heat shock at 42°C for 1.5 min and quickly chilled on ice for 2 min. For electroporation, DNA/competent cells mixture was pipetted into the cuvette and electroporated using the Gene Pulser apparatus (Biorad) at 25Mfd, 200Ω and 1.8kV. Subsequently 1 ml of LB medium was added in the cells prior to incubation at 37°C for 1h with shaking at

200 rpm. For ligation mixture, the whole pellet after centrifuge, while for plasmid about 100 µl of the transformation mix was sprayed onto selection plates with appropriate antibiotics.

2.4.6 Purification of plasmids from bacteria in a small scale

Single bacterial colony was inoculated into 2ml of LB medium containing the appropriate antibiotics. The LB culture was incubated at 37°C with vigorous shaking (250rpm) for overnight. About 1.5 ml of the overnight culture was transferred into a microfuge tube and centrifuged at 4500rpm for 3 min, followed by purification with the Qiagen QIAprep Miniprep Kit according to the manufacturer's instructions.

2.4.7 Screening of transformants by restriction digestion and DNA sequencing

The extracted plasmids from picked colonies were digested with the same restriction enzymes as before ligation reaction. The correct colonies were identified by checking suitable insert bands in agarose gel loaded with digestion product. The plasmids with correct insert bands then were processed for sequencing.

Sequencing reaction was set up for 10 µl of volume containing 0.25 µg of DNA template, 1.6 ρmol of primer, and 4 µl of BigDye terminator reaction mixture (ABI PRISM TM Dye terminator Cycle Sequencing Ready Reaction Kit). The cycle sequencing was performed on the GeneAmp PCR as follows: 25 cycles of 96°C for 10 sec, 50°C for 5 sec, 60°C for 4 min; rapid thermal ramp to 4°C and hold. The reaction product was purified by ethanol precipitation then applied to the ABI PRISM 3100 automated sequencer. DNA sequences were determined on both strands of the cDNA

clone.

2.5 *Agrobacterium* transformation of *Arabidopsis*

See Table 2A for a list of binary plasmids used in this study. *Arabidopsis thaliana* (*Col-0*) plants were transformed by *Agrobacterium* (EHA105 strain)-mediated infiltration using the floral dipping method (Clough and Bent 1998; Zhang et al. 2006). After the recombinant plasmid was transformed into *Agrobacterium tumefaciens* strain EHA105 by electroporation, the *Agrobacterium* stain carried the recombinant plasmid was grown overnight at 28℃ 200rpm. 2ml of overnight-cultured *Agrobacterium* was inoculated into 200ml of LB medium supplemented with antibiotics (50mg/L kanamycin and 25 mg/L rifampicin) and 10μM of acetosyringone (AS). The pH was adjusted to 5.6 using potassium hydroxide (KOH). The culture was grown overnight at 28 ℃ and 200 rpm. *Agrobacterium* cells were then harvested by centrifugation at 4000 rpm/ 4 ℃ at for 10 minutes and resuspended with 5% fresh sucrose solution to final OD 600 of 1.5. Finally, before dipping, Silwet-L 77 was added to the sucrose solution with the final concentration about 0.02% (v/v).

Seeds of T_0 generation from dipped plants were selected by germination on MS medium (Sigma) with 50μg/ml kanamycin. Successful transformants (T1 plants) were generated and grown in soil. Transformation efficiency is about 1%. The presence of *AK6b* or its mutant's transgene was detected in the T_1 plants by PCR using the following primers including a part sequence of 35S promoter:

35S-F: GTCTCTTACGACTCAATGACAAG

AK6b-R: CCTCAACATAATTACCTAGCCT

All plants were grown in a growth chamber with a cycle of 14hr light at 22^{o}C and 10hr dark at 18^{o}C.

2.6 Nuclei acid isolation and Reverse transcription (RT)-PCR

Genomic DNA was isolated from *Arabidopsis* leaves using the Cetyltrimethylammonium bromide (CTAB) method described by Doyle et al. (1990). Briefly, 0.3 g of leaf tissues was ground in 600 µl of 2% CTAB buffer (2% CTAB, 0.1 M Tris-HCl, pH 8.0, 1.4 M NaCl, 20 mM EDTA and 0.2% β-mercaptoethanol) and the homogenate was incubated at 60°C for 1 hour with constant mixing. Chloroform/isoamyl alcohol mixture (24:1, v/v) (500µl) was added to the homogenate followed by centrifugation at 14,000 rpm and 4°C for 15 minutes. The aqueous layer (500µl) was transferred to a new microfuge tube containing 500 µl of cold isopropanol and was kept at -20°C for 1 hour. The DNA pellet was precipitated by centrifugation and washed with 75% ethanol. After 5 minutes of vacuum drying, the pellet was resuspended in distilled water. Total RNA was extracted from *Arabidopsis* leaves by TRIZOL reagent (Invitrogen) according to the manufacturer's protocol.

Reverse transcription (RT)-PCR reaction was set up according to the instructions of Titan one tube RT-PCR system (Roche Molecular Biochemicals). Master mix 1 was set up to 25 µl containing 0.2 mM of each dNTP, 0.4 µM of upstream primers, 0.4 µM of downstream primers, 5 mM of DTT solution, 5 units of RNase inhibitor and 0.1µg of total RNA. Master mix 2 was set up to 25 µl including 1.5 mM $MgCl_2$, 1× RT-PCR

buffer and 1 μl of enzyme mix. Mix 1 and mix 2 were added together and mixed properly, the mixture was placed in a thermocycler equilibrated at 50°C and incubated for 30 min, then applied to thermocycling at 94°C for 2 min to denature template; 10 cycles of denaturation at 94°C for 30 sec, annealing at 45-65°C (based on the melting temperature of primers used) for 30 sec and elongation at 68°C for proper time; 25 cycles of denaturation at 94°C for 30 sec, annealing at 45-65°C (based on the melting temperature of primers used) for 30 sec and elongation at 68°C for proper time, adding cycle elongation of 5 sec for each cycle; finally prolonged elongation time up to 7 min at 68°C.

2.7 Protein expression and purification

2.7.1 Induction of protein expression in bacteria

A fresh bacterial colony harboring the expression plasmid was inoculated into 100 ml of 2×YT medium containing 100 μg/ml antibiotics. After overnight incubation at 37°C with shaking, the 100 ml bacteria culture was diluted into 8L of fresh 2×YT medium containing the same antibiotics, and was grown at 37°C with vigorous shaking (250rpm) until the OD600 reached 0.6. The expression of the desirable protein was induced by adding IPTG to a final concentration of 0.4 mM, and the culture was incubated at 37°C with vigorous shaking for 4 h or at 22°C overnight. The bacterial cells were harvested by centrifugation at 4,000 rpm for 15 min, and the pellet was stored at -20°C for further purification.

2.7.2 Protein purification

His tag or His-SUMO tag fusion proteins included His- (AK6b, AB6b, SE) and His-SUMO-H3. Such kind of proteins was purified with Ni^{2+} NTA column (5ml, GE healthcare). The column was equilibrated with native purification or binding buffer (50mM NaH_2PO_4, pH 8.0, 500mM NaCl). Then the lysate was loaded to Ni^{2+} NTA column at 1ml/min. The column was washed with native purification or binding buffer and further washed with native wash buffer (50mM NaH_2PO_4, 500mM NaCl, 20 mM imidazole, pH 8.0). After that his-tag fused protein was eluted from the column by native elution buffer (50mM NaH_2PO_4, 500mM NaCl, 250 mM imidazole, pH 8.0). The peak fractions was pooled together and dialysis against to native purification or binding buffer. The 6xHis-tag from the fusion protein was removed by using the specific protease.

GST- tagged proteins included GST- AK6b, -AB6b, -AK6b (Δ200-208), -SE-Mid and -SE-NT. The GST-fused protein was purified with the glutathione sepharose affinity column. After centrifugation for harvesting the bacteria which contains the expressed target protein, cells were resuspended in 1×PBS (140mM NaCl, 2.7mM KCl, 10mM Na_2HPO_4, 1.8mM KH_2PO_4 (pH 7.3), with complete proteinase inhibitor (Roche). The resuspended bacteria or the thawy bacteria pellet from storage at -20°C was lysed by cell disruptor. After centrifugation (40,000 g, 1 hr), the supernatant was loaded onto a glutathione sepharose affinity column equilibrated in 1×PBS. Nonspecific binding proteins were washed out by 1×PBS buffer and the fused protein was eluted by elution buffer (0.154g reduced glutathione dissolved in 50ml 50mM Tris-HCl, pH8.0). Pooled fractions from the glutathione sepharose affinity column

were concentrated and if need the N-terminal GST-tag was cleaved by PreScission protease or Thrombin before loaded on a HiLoad Superdex G-75 column (GE healthcare) equilibrated in 500 mM NaCl, 10 mM DTT, and 25 mM Tris, pH 7.4 for further purification. The peak fractions from the Superdex G-75 were pooled together and concentrated in a Microcon (Amicon).

MBP tag fusion proteins included MBP, MBP-AK6b (Δ40-55), -AK6b (Δ164-184), -AGO1-PolyQ, -AGO1-NT, -AGO1-PAZ, -AGO1-Mid, -AGO1-PIWI1 and -AGO1-PIWI2. The MBP-fused protein was purified by affinity chromatography on amylose matrices. An N-terminal MBP fusion can increase the solubility of a protein. The maltose binding protein, connected via a short linker to the N-terminus of the desired protein, binds to the amylose resin. The protein can be eluted by competitive displacement with maltose. For the following pull-down assay, the MBP-tag was kept and no need to be cleaved with Factor Xa protease.

2.7.3 Sodium dodecylsulfate-polyacrylamide electrophoresis (SDS-PAGE)

SDS-polyacrylamide gel was consisted of 12% separating gel (1.6 ml water, 2.0 ml 30% acrylamide, 1.3 ml 1.5 M Tris.Cl (pH 8.8), 50 µl 10% SDS, 50 µl 10% ammonium persulphate (APS), 2 µl N,N,N',N'-Tetramethylethylenediamine (TEMED)) in the bottom and 5% stacking gel (1.36 ml water, 333 µl 30% acrylamide, 250 µl 1M Tris (pH 6.8), 20 µl 10% SDS, 20 µl 10% APS, 2 µl TEMED) in the upper. The samples were treated with equal volume of loading buffer (0.1 M Tris-HCl, pH 6.8, 20% glycerol (V/V), 4% SDS (W/V), 5% β-mercaptoethanol (V/V), 0.2% bromophenol blue (W/V)) at 100 °C for 4 min. The running buffer (pH 8.3) contained

the following reagents in a volume of 1 liter: 94 g glysine, 25 ml 10% SDS and 15.1 g Tris-base. The electrophoretic unit was supplied with 120 V for 45-90 minutes.

2.8 Protein crystallization

2.8.1 Light scattering

Dynamic light scattering in DynaPro99 Molecular Size Instrument was used for checking the homogenous quality of protein sample before crystal growth. The procedures are operated according to user manual. Briefly, clean the cuvettes before and after use with water and ethanol then dry the cell using "air-it", make sure the cuvette is clean, inject the filtered sample into the cuvette for testing and analysis under the Dynamics program on the computer.

2.8.2 Hanging drop crystallization

Crystallization conditions were screened by the hanging-drop vapour-diffusion method using 24 wells crystallization plates (Hampton Research, Laguna Niguel, CA, USA). The drops were set up with 1ul of purified protein and 1ul of crystallization well buffer. The 1 ml reservoir buffers in well were taken from Hampton, Qiagen, Crystalgen, Wizard (Emerald Biosystem), Crystallization and TOPAZ crystal screen kits. Crystallization trials were set up at 288 K. Conditions that gave crystalline precipitates in the hanging drops were identified and optimized further.

Crystals of AK6b were grown by hanging drop vapor diffusion at 20 ºC. Typically, a 2 µl hanging drop contained 1.0 µl of protein (15 mg/ml) mixed with 1.0 µl of reservoir containing 0.3M magnesium formate and 0.1M Bis-tris buffer, pH5.9, then

equilibrated over 1ml of reservoir solution. The crystals grew to a maximum size of 0.2 mm×0.2 mm×0.1 mm over the course of 2 days.

Crystals of AB6b were grown by hanging drop vapor diffusion at 20 ºC. Typically, a 2µl hanging drop contained 1.0µl of protein (10 mg/ml) mixed with 1.0µl of reservoir containing 0.35M ammonium dehydrate phosphate and 0.1M sodium citrate, pH5.8, then equilibrated over 1ml of reservoir solution. These crystals grew to a maximum size of 0.05 mm×0.05 mm×0.02 mm over the course of 7 days.

2.9 Data collection

Cryoprotectant trials were processed to find suitable cryoprotectant for picking up and flash freezing crystals in liquid nitrogen. Crystals were soaked in ascending concentrations of cryoprotectant (increments of 5% from 5 to 30%) in glass cover to find suitable concentrations of cryoprotectant.

When collecting diffraction data, a total of 360 frames of 1º oscillation were collected for each crystal on beamlines at the National Synchrotron Light Source at Brookhaven National Laboratory and the data was processed by HKL2000 (www.hkl-xray.com).

For data collection, AK6b crystals were flash frozen (100K) in the above reservoir solution supplemented with 30% glycerol. A total of 360 frames of 1º oscillation were collected for each crystal per wavelength. Total 3 wavelengths data were collected corresponding to selenium peak (0.9790Å), inflection (0.9794Å) and remote (0.96Å), respectively. The data was collected on beam line X12C at the

National Synchrotron Light Source at Brookhaven National Laboratory and was processed by HKL2000 (www.hkl-xray.com). The crystals belong to space group $P3_221$, with unit cell parameters listed in Table 1.

AB6b crystals were flash frozen (100K) in the reservoir solution supplemented with 30% glycerol. A total of 360 frames of 1º oscillation were collected at wavelength 1.1Å on beam line X29 at the National Synchrotron Light Source at Brookhaven National Laboratory and was processed by HKL2000 (www.hkl-xray.com). The crystals belong to space group $P2_12_12$, with unit cell parameters listed in Table 1.

2.10 Structure Determination

The crystal structure of AK6b was determined by multiple wavelength anomalous dispersion (MAD) using SOLVE/RESOLVE (www.solve.lanl.gov) and the MAD phase was calculated and improved by density modification assuming a solvent content of ~48% using the SHARP program (www.globalphasing.com). The crystal structure of AB6b was determined by molecular replacement with AK6b structure as the search model. The models were built by using the program O and refined using REFMAC/CCP4. The R-free set contained 5% of the reflections chosen at random. The model comprises residues XX-XXX (AK6b) or XX-XXX (AB6b). Disordered region, including loop segment XX-XX (AK6b) or XX-XX (AB6b) was not included in the model.

2.11 *In vitro* pull-down assays

Fifty micrograms of His-tagged target proteins were pre-absorbed for 1 h at 4 °C in 1 ml of binding buffer, including 50 µl Amylose resin (Biolabs) or Glutathione agarose beads (GE Healthcare), 50 mM Tris-HCl, pH 7.5, 100 mM NaCl, 0.2% NP-40, 0.6% Triton X-100. The mixture was cleared by centrifugation at 12,000 g for 2 min. The resulting supernatant was transferred to a fresh tube containing 30 µl Amylose Resin beads or Glutathione Sepharose beads. After incubation for 2h at 4 °C, 50 µg of the MBP-tagged or GST-tagged bait proteins were added and the incubation continued under the same conditions overnight. Finally, after vigorous washes for 6 times, pulled-down proteins were resolved by SDS-PAGE and detected by western blot.

2.12 Co-immunoprecipitation experiments

For co-immunoprecipitation experiments, total proteins were extracted from two-week-old *35S::AK6b* transgenic *Arabidopsis* seedlings in 50 mM Tris-HCl, pH 7.5, 150 mM NaCl, 10 mM MgCl2, 0.2% 2-mercaptoethanol, 0.2% Triton-100 and 5% Glycerol supplemented with a EDTA-free protease inhibitor cocktail (Amersham Pharmacia). Protein extracts were immunoprecipitated with purified polyclonal antibody to AK6b at 4°C for 2 h. Protein A beads were then added and incubated overnight. Beads were washed 6 times with the same buffer before an equal volume of 2x SDS-loading buffer was added. Western blots were analyzed with a polyclonal antibody specific to SE or H3 to detect co-immunoprecipitated proteins.

2.13 Western blot analyses

Protein samples were seperated on SDS-polyacrylamide gel. For transferring proteins to PVDF membrane (Roche Diagnostics GmbH, Germany), the membrane was soaked in methanol and transfer buffer (10% methanol, 0.01 M Tris.base, 0.096 M glysine) for 10 min, respectively. The apparatus was supplied with 100 V for 1 h. The membrane with proteins was then transferred into blocking buffer (5% non-fat milk powder in TBST (10 mM Tris.Cl, pH 8.0, 150 mM NaCl, and 0.05% Tween 20)) and the membrane was kept at 4°C overnight with gentle shaking.

Primary antibody was added into 10 ml TBST buffer and the mixture together with membrane was shaken for 1 h at room temperature. Secondary antibody (1:10,000 diluted in TBST) was added to the membrane and incubated at room temperature for 40 min. The membrane was washed with TBST for 10 min for three times before and after adding antibodies. Then the membrane was put on the film that was developed in dark till bands were clearly visible.

2.14 Northern blot analysis

For analysis of miRNAs, total RNA was separated on denaturing 15% TBE-Urea gels and transferred onto BrightStar- Plus positively charged nylon membranes (Ambion). After UV CrossLink for 2 min, the membranes were prehybridized at 42°C for 0.5 h using Ultrahyb-Ultrasensitive Hybridization Buffer (Ambion) and subjected to hybridization with Biotin-labeled miR162, miR164, and miR165/166 or miR319 probes overnight at 42°C. Following hybridization, membranes were initially rinsed

and then washed 2×5min 2XSSC, 0.1% SDS at 42°C, then followed by washing 2×15min 0.1XSSC, 0.1% SDS at 42°C. Probe detection was performed using LightShift Chemiluminescent EMSA Kit (Thermo Fisher Scientific Inc., USA) according to manufacturer's protocol. In brief, blots were incubated in blocking solution for 30 min and then in antibody solution (anti-biotin, Streptavidin conjugated antibody) for 30 min, followed by washing five times in washing buffer. After equilibration in the Substrate Equilibrate buffer for 5min, blots were completely covered by the Substrate Working Solution and exposed to Kodak Biomax MR film.

miRNA probe sequences selected based on published sequences listed in the miRNA Registry (http://www.sanger.ac.uk/Software/Rfam/mirna/) are as follows:

miR162: 5'-CTGGATGCAGAGGTTTATCGA-3'

miR164: 5'-TGCACGTGCCCTGCTTCTCCA-3'

miR165/166: 5'-GGGGGATGAAGCCTGGTCCGA-3'

miR319: 5'- AGGGAGCTCCCTTCAGTCCAA -3'.

The 5'-Biotin-labeled DNA oligonucleotides were purchased and synthesized by 1st Base Pte Ltd (Singapore).

2.15 Real-time RT-PCR

Total RNA was isolated from the aerial parts of 20d-old wild-type and *se-1* and *35S::AK6b* seedlings using Trizol reagent (Invitrogen). Reverse transcription was performed with 2μg total RNA using Titan one tube RT-PCR system (Roche Molecular Biochemicals) PCR was carried out in the presence of the double-stranded

DNA-specific dye SYBR Green (Applied Biosystems, Warrington, UK). Amplification was monitored in real time with the 7500 Real Time PCR System (Applied Biosystems, Warrington, UK). PCR was carried out with the following gene-specific primers:

CUC1: 5'- CAACGGGACTGAGAACGAACA -3'

5'- CGGTGGAGCGGGAAGGAAT -3'

DCL1: 5'- GGTGTCACTCTTGCAATGT -3'

5'- CCTGGCTGTTATTGTGTC - 3'

NAC1: 5'- GGTAAGCTAGTTGGGATGAG - 3'

5'- CAGAGACTGAGTTGGTTAGGT - 3'

REV: 5'- ATCTGTGGTCACAACTCC - 3'

5'- TAGCGACCTCTCACAAAC -3'

TCP4: 5'- CGCTGCTAACGCTAAAC -3'

5'- TGTTGGTGGTGCAGAAG - 3'

ACTIN: 5'- TGGCATCACACTTTCTACAA - 3'

5'- CCACTGAGCACAATGTT - 3'

For real-time PCR, quantifications of each cDNA sample were made in triplicate, and the consistent results from at least two separately prepared RNA samples were used. For each quantification, conditions were, as recommended, $1 \geq E \geq 0.80$ and $r^2 \geq 0.980$, where E is the PCR efficiency and r^2 corresponds to the correlation coefficient obtained with the standard curve. Results were normalized to that of *ACTIN*. The PCR products were then analyzed by gel electrophoresis, and the relative abundance of

gene transcripts was calculated using the first-lane product from wild-type cDNA as 1.0.

2.16 Transient Expression of Fluorescent Protein Fusions in Onion Cells

For the transient expression assays of *AK6b-CFP, SE-YFP or AGO1-YFP* chimeric gene, the pBA002/35S::AK6b-CFP plus pBA002/35S::SE-YFP or the pBA002/35S::AK6b-CFP plus pBA002/35S::AGO1-YFP plasmid was introduced into onion cells by particle bombardment. Fresh onion bulbs were cut into slices of 1 cm^2 and placed on the central area of a petri dish with 0.9% phytal agar as supporting medium. Tungsten particles of 1.0 μm in diameter were prepared and coated with plasmid DNA according to BioRad's protocol. Bombardments were performed using the Biolistic PDS-1000/He Particle Delivery System (BioRad) with the following parameters:

Holder level: 2

Sample level: 4

Gap distance: 0.63 cm

Target distance: 6 cm

Helium pressure: 1100 psi

Chamber vacuum: 27 inches Hg (~ 0.06 atm)

Amount of DNA/bombardment: 1μg

Amount of macrocarrier/bombardment: 500 μg of tungsten particle

Each sample received two times of bombardment, after which the samples were

kept in the dark at room temperature for 24 h before analysis by confocal microscopy (LSM 510 microscope; Zeiss, Jena, Germany). YFP fluorescence was imaged using excitation with the 514-nm line of the argon laser and a 530-nm band-pass emission filter, and CFP fluorescence was imaged using excitation with the 458-nm line of the argon laser and a 475- to 525-nm band-pass emission filter. Imaging of YFP and CFP was performed sequentially. Samples were scanned with the Z-stack mode, and the projection of the image stacks was calculated with the LSM 510 microscope's three-dimensional functions.

Signals from both channels corresponding to each image were compared using Adobe Photoshop 6.0 (Mountain View, CA), and the results shown in the merged columns indicate protein colocalization.

Chapter 3 Results

3.1 Expression and purification of 6b proteins

Before protein expression, a sequence comparison between the three 6b protein (AK6b, AB6b and T6b) and RolB is shown in Figure 1. The CLUXTAL W multiple sequences alignment program (Thompson et al., 1994) was used for this analysis. The result shows that the 6b proteins have high identity, especially between AK6b and AB6b, while the RolB sequence shows low identity to the three 6b proteins. Figure 1 also shows the secondary structure of the proteins.

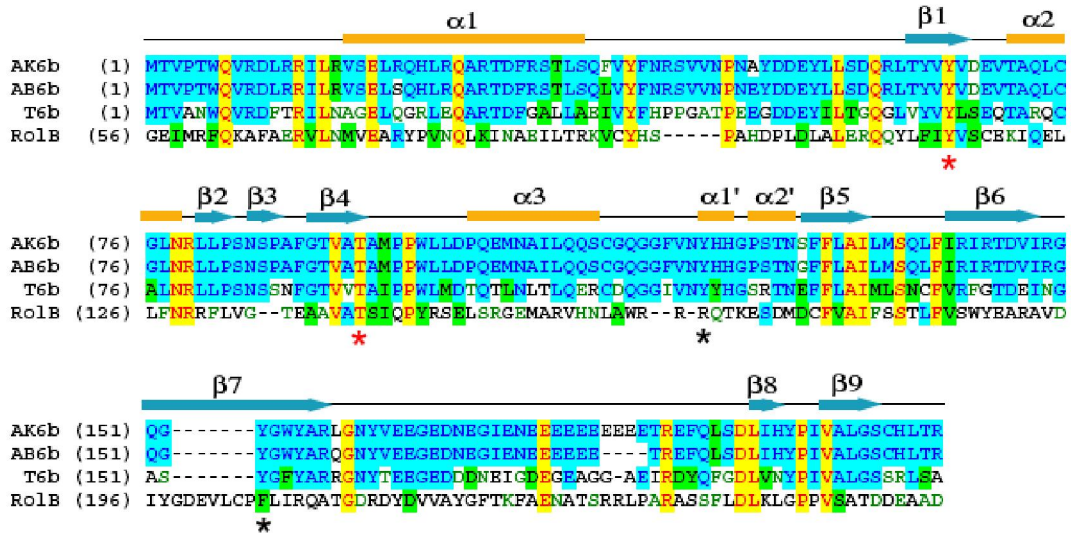

Fig. 1 Sequence alignment of 6b genes with RolB.

The aligned sequences are in the order of *Agrobacterium tumefaciens* AK6b, *Agrobacterium vitis* AB6b, *Agrobacterium vitis* T6b and *Agrobacterium rhizogenes* RolB. The secondary structure diagram for AK6b is shown on the top. Alpha helices are colored in yellow and β-strands in green. Conserved residues are shaded in cyan (80% similarity) and green (60% similarity), whereas essentially invariant residues in yellow.

As shown in Fig.2 and Fig.3, both AK6b and AB6b full length proteins fused with Nhis-tag (totally about 27kDa) were successfully expressed in soluble form, purified through Ni^{+} NTA column (Fig. 2A and 3A) and gel filtration column superdex G75 (Fig. 2B and 3B).

(A)

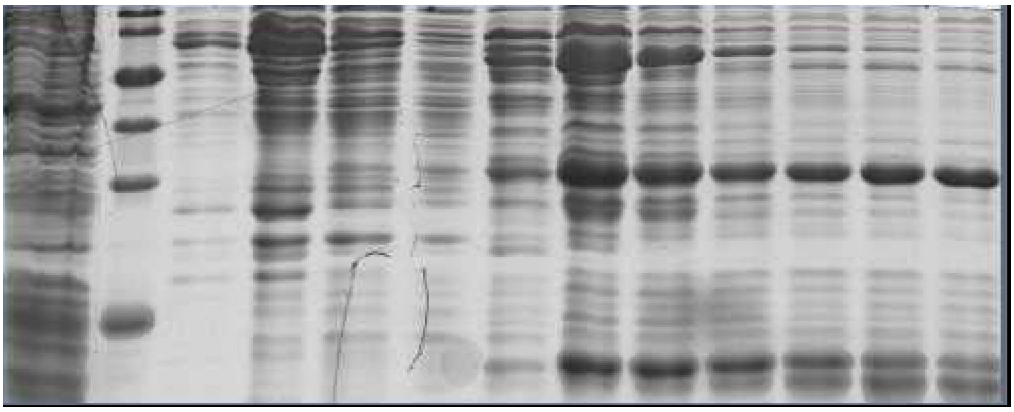

(B)

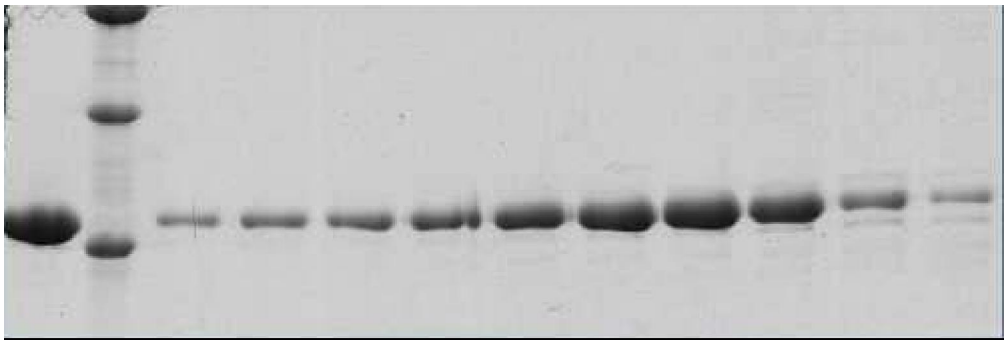

Fig. 2 Expression and purification of AK6b protein.

(A) Expression of AK6b full length fused with N-terminal his-tag and purification through HisTraptm HP column. M, Perfect protein marker; lane1, the flow through after passing through the column; lane 2-5, fractions eluted at 25 mM imidazole; Lane 6-12, AK6b protein eluted at 250 mM imidazole; (B) Purification through gel filtration column; M, Perfect protein marker; Lane1-10, fractions.

(A)

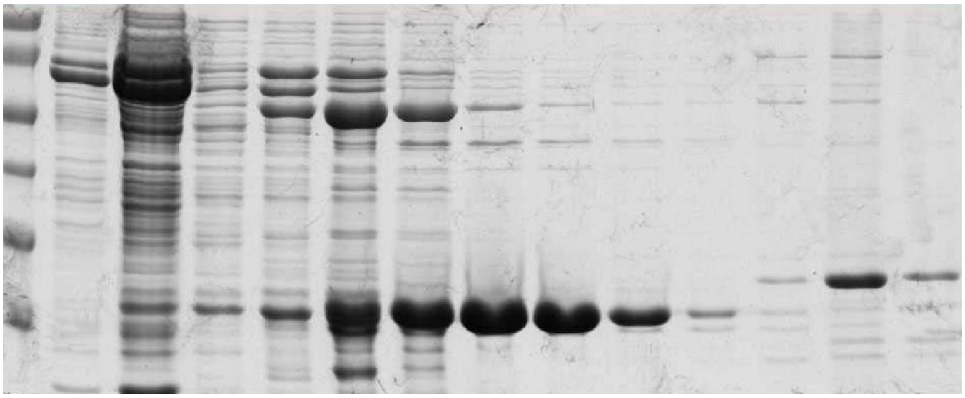

(B)

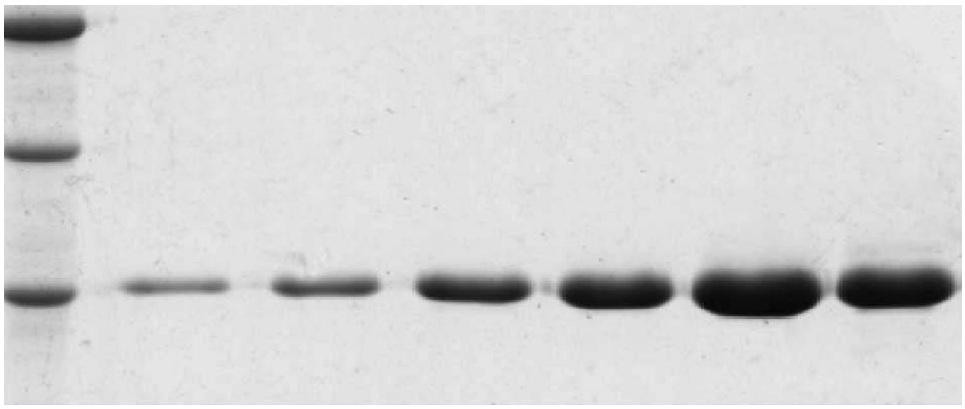

Fig. 3 Expression and purification of Nhis-AB6b Protein.

(A) Expression of AB6b full length fused with N-terminal his-tag and purification through HisTraptm HP column. M, Perfect protein marker; lane 1-4, fractions eluted at 25 mM imidazole; Lane 5-10, AK6b protein eluted at 250 mM imidazole; Lane 11-13, fractions eluted at 500 mM imidazole (B) Purification through gel filtration column; M, Perfect protein marker r; Lane1-6, fractions.

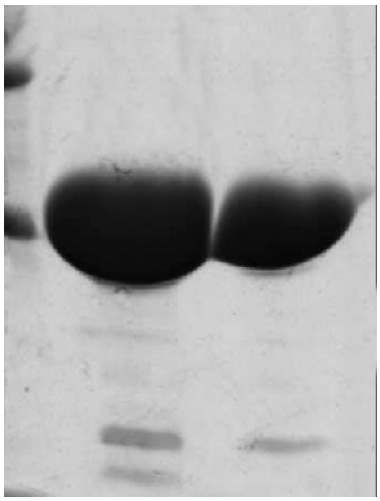

Fig. 4 15% SDS-PAGE of purified AK6b and AB6b used for crystallization.
M: perfect protein marker, Lane 1: AK6b, Lane 2: AB6b.

For crystallization, the protein concentration was about 10-15 mg/ml (Fig. 4). Crystals were grown by hanging drop vapor diffusion at 20 ºC. Typically, 2.0 µl hanging drop contained 1.0 µl of protein mixed with 1.0 µl of reservoir and equilibrated over 1 ml of reservoir solution. For AK6b, the crystals were grown in the reservoir contained 0.3 M Magnesium Formate and 0.05 M Bis-tris (pH5.9). For AB6b, the reservoir contained 0.35M Ammonium Dihydrate Phosphate and 0.05 M Sodium Citrate (pH5.8) These crystals grew to a maximum size of about 0.1 mm×0.05 mm×0.05 mm as clusters over the course of 2-5 days (Fig. 5 and Fig. 6).

For data collection, crystals were flash frozen (100K) in the above reservoir solution supplemented with 30% glycerol. A total of 360 frames of 1º oscillation were collected for each crystal on beamline X12C at the National Synchrotron Light Source at Brookhaven National Laboratory and was processed by HKL2000 (www.hkl-xray.com). From the analyses of the diffraction pattern (Fig. 7 and Fig. 8), the crystals were found belong to space group $P3_221$ and $P2_12_12$, respectively, with unit cell parameters listed in Table 1.

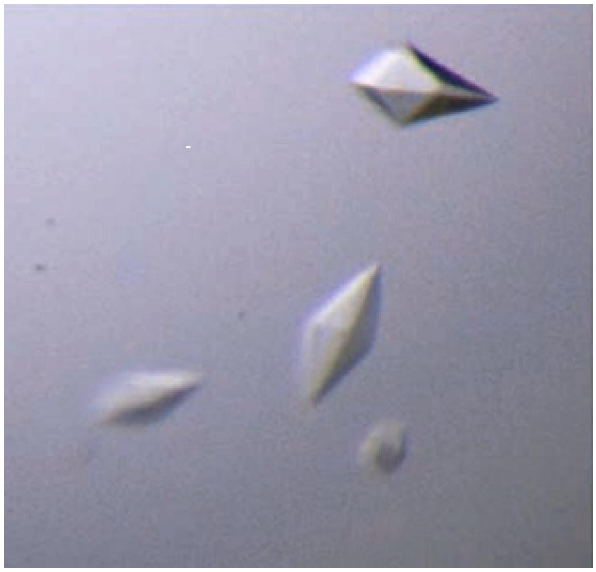

Fig. 5 Image of AK6b crystals (40X magnification).

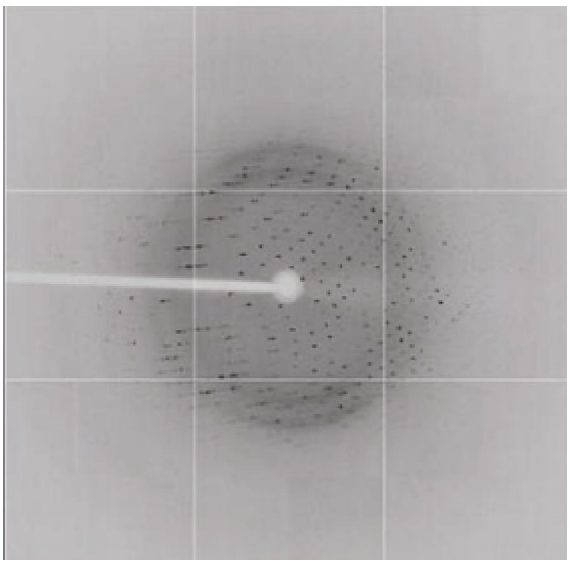

Fig. 6 Diffraction pattern from a well-formed AK6b crystal.
AK6b crystal diffracted to 2.1Å with good mosaicity and acceptable Rmerge.

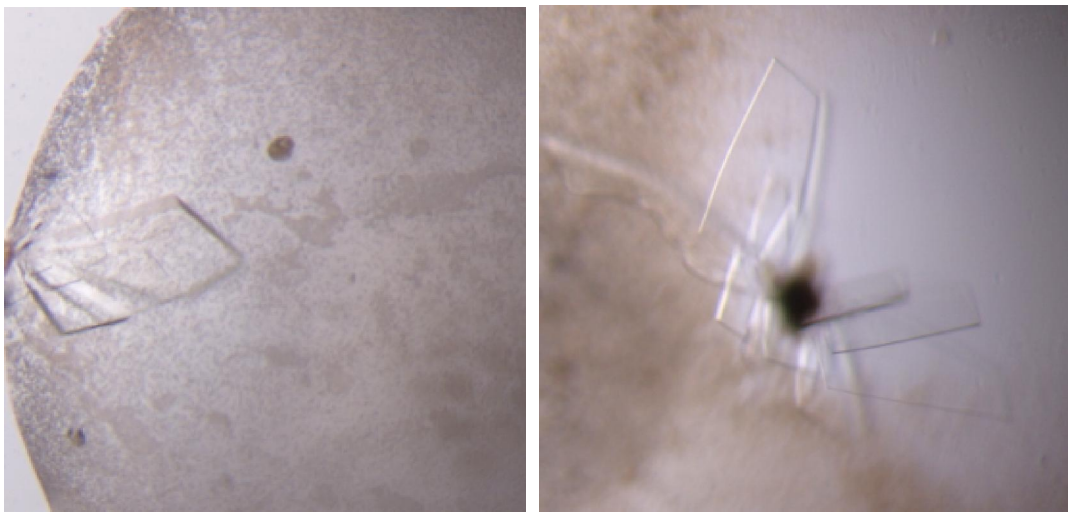

Fig. 7 Image of AB6b crystals (40X magnification).

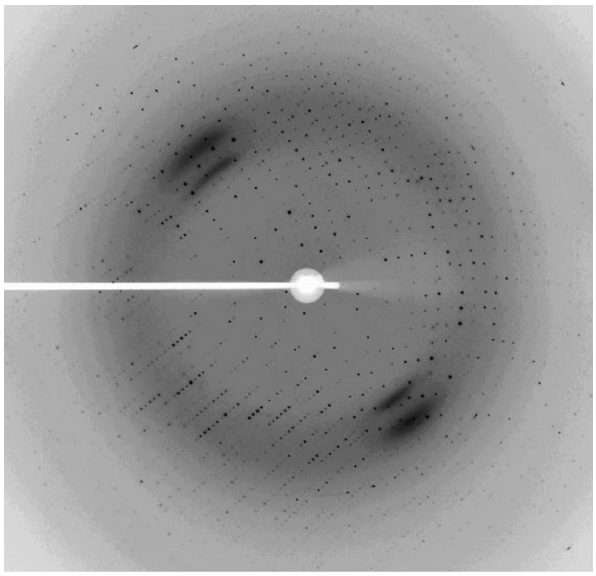

Fig. 8 Diffraction pattern from a well-formed AB6b crystal.
AB6b crystal diffracted to 1.65Å with good mosaicity and acceptable Rmerge.

Table 1 Data collection, phasing and refinement statistics

Data collection		AK6b		AB6b
Space group		$P3_221$		$P2_12_12$
Molecules/ASU		3		2
Data set	Peak	Inflection	Remote	Native
Cell dimensions				
a (Å)		80.458		79.366
b (Å)		80.458		89.926
c (Å)		245.708		59.583
Wavelength (Å)	0.9790	0.9794	0.96	1.1
Resolution (Å) [a]	50~2.1 (2.18~2.10)	50~2.1 (2.18~2.10)	50~2.1 (2.18~2.10)	50~1.65 (1.68~1.65)
R_{sym} (%)	7.4 (35.4)	7.4 (36.0)	8.2 (42.3)	7.3 (52.1)
$I/\sigma(I)$	30.3/2.8	27.9/2.7	22.8/1.3	44.8/4.0
Completeness (%) [a]	81.1 (32.9)	74.6 (21.8)	66.0 (12.9)	99.9 (99.6)
Redundancy	9.7 (4.4)	9.7 (3.7)	7.7 (7.3)	13.9 (10.5)
Initial Figure of Merit		0.5		
Refinement				
Resolution Range (Å)	50~2.1			50~1.65
No. reflections	43,896			49,396
R_{work}/R_{free} (%)	20.2/23.7			17.8/20.6
No. atoms				
Protein	4,588			3,046
Water	258			342
B-factors ($Å^2$)				
Protein	39.8			17.7
Water	38.7			34.2
R.m.s. deviations				
Bond lengths (Å)	0.010			0.009
Bond angles (°)	1.18			1.15
% favored (allowed) in Ramachandran plot	90.3 (9.7)			92.4 (7.6)

[a] Values for the highest-resolution shell are in parentheses.

3.2 Overall Crystal structures of AK6b and AB6b

Crystal structure of the full-length *Agrobacterium tumefaciens* AK6b at 2.1 Å was solved by multiple anomalous dispersion (MAD) phasing, whereas *Agrobacterium vitis* AB6b at 1.65 Å was determined by molecular replacement (AK6b as the search model), with crystallographic statistics summarized in Table 3. AK6b and AB6b have very similar sequences and almost identical structures, except that AB6b harbors a little shorter repeating Glu residues loop in the middle. Therefore, hereafter we will use the generic name 6b to represent both AK6b and AB6b proteins and the amino acid residue numbers from AK6b.

6b contains nine β-strands (β1- β9), three regular α-helices (α1- α3) and two very short α-helices (α1'- α2') (Fig. 1) and possesses a α/β fold with five α-helices packed against nine β-strands at one surface with an overall dimension of 50Å×35Å×25Å. The 6b central module contains two perpendicular β-sheets (β1, β2, β5, β8 and β9 forming one group, whereas β3, β4, β6 and β7 forming another group) and one α-helix (α2) sitting on top of these two β-sheets, surrounded by several loops and two α-helices (α1 and α3) (Fig. 9).

A well ordered loop (residues: 113-134), including the two very short α-helices (α1' and α2'), connecting α3 and β5 forms a lid-like architecture covering the central structural module formed by perpendicular β-sheets. Another well ordered 17-amino acid long loop (residues: 40-55) connecting α1 and β1 extends from the central module of the structure. This loop participates in protein packing and may serve as a structural scaffold for protein-protein interaction. The well-studied loop with

repeating Glu residues (ten Glu residues for AK6b and six Glu residues for AB6b) is disordered in both AK6b and AB6b structures (Kitakura, et al., 2002; Kitakura, et al., 2008).

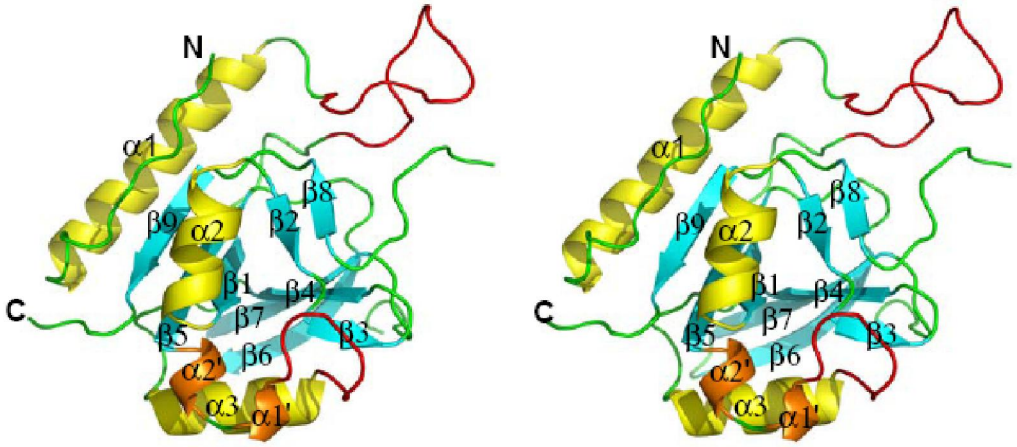

Fig. 9 Overall structure of *Agrobacterium* protein 6b.
Stereoview ribbon representation of 6b with two extended loops colored in red.

3.3 6b shares structural similarities with ADP-ribosylating toxins

At a first step towards investigating investigate the molecular mechanism for 6b-mediated gene regulation; 3D structure homolog search was performed by using a Dali server (www.ebi.ac.uk/dali). Surprisingly, the central module of the 6b structure including the two perpendicular β sheets and the closely packed α helix (α2) shows close structural homology to those of the Exotoxin A central module (PDB: 1XK9, Z score 4.1, r.m.s.d. 4.0.X Å, 100 Cα) (Yates, et al., 2005) and Cholera toxin central module (PDB: 1S5C, Z score 3.4, r.m.s.d. 3.5 Å, 86 Cα) (O'Neal, et al., 2004) (Fig. 10A), In spite of the lack of any apparently sequence similarities amongst them. Notably, both Exotoxin A and Cholera toxin belong to ADP-ribosylating toxins with

the ADP-ribotransferase fold (Deng and Barbieri, 2008).

However, there are significant structural differences amongst 6b, Exotoxin A and Cholera toxin, not only at the structural motifs surrounding the central modules but also within the central modules. In general, 6b adopts a more compact globular fold with more secondary structure features, whereas both Exotoxin A and Cholera toxin have a loose fold and less structural features within the central modules. Remarkably, 6b central module is closer to that of Cholera toxin, both of them having only one α-helix on one side and lacking the second α-helix on the other side (Fig. 10A). More important, the putative NAD^+ substrate-binding pocket, characterized by Exotoxin A, is closed by an active-site loop both at the 6b and Cholera toxin structures, whereas the substrate-binding pocket is opened at the Exotoxin A structure (Fig. 10B). Hence, the substrate-binding pocket within 6b is not accessible to the substrate or other proteins. Therefore, significant conformational changes are required for 6b to open this pocket.

To obtain evidence that 6b protein harbors the NAD^+ binding pocket, 35S promoter driven 6b overexpression transgenic plants (*35S::AK6b*) in the *Col-0* background were treated with different amount of NAD^+ inhibitor, thiazole-4-carboxamide adenine dinnucleotide (TAD). As expected, the morphological phenotypes accompanying with 6b overexpression, such as leaf serration, were gradually rescued with the addition of increasing amounts of TAD (Fig. 11).

3.4 Putative NAD^+ binding site of 6b

Despite the apparently divergent sequences amongst 6b and ADP-ribosylating toxins, 6b does share an overall structural similarity at its putative NAD^+ binding pocket (Fig. 12A). In addition to the structural conserved central module mainly formed by perpendicular β-sheets that serves as the NAD^+ binding pocket, 6b also contains a conserved α-helix (α3) underneath the putative NAD^+ binding pocket (Fig. 12A). However, there is neither absolutely conserved glutamic acid residue on one side of the pocket nor conserved histidine (Exotoxin A) nor arginine (Cholera toxin) on the opposite side of the pocket (Fig. 12A, 12B). By contrast, the absolutely conserved glutamic acid on ADP-ribosylating toxin is replaced by the invariable Tyr153 residue, the conserved histidine or arginine residue is replaced by Tyr66, whereas the conserved Tyr470 and Tyr481 residues on Exotoxin A or Ser61 and Arg11 residues on Cholera toxin are replaced by conserved Thr93 and Tyr121 residues (Fig. 12B).

Similar to the Exotoxin A, the aromatic ring cage environment created by Tyr121, Tyr153, Tyr156 and Tyr121 probably participates in NAD^+ binding for anchoring the nicotinamide ring of NAD^+. Tyr66 may also stabilize NAD^+ binding by forming a hydrogen bond with the bound NAD^+, whereas the Thr93 side chain probably forms a hydrogen bond to the putative catalytic Y153 residue (Figure 12B).

Similar to other bacterial ADP-ribosylating toxins, 6b structures also share two crucial features around the NAD^+ binding pocket: the active-site loop and the ARTT motif (ADP-ribosylating toxin turn-turn motif), which consists of residues from two

adjacent protruding turns (Deng and Barbieri, 2008) (Fig. 12A).

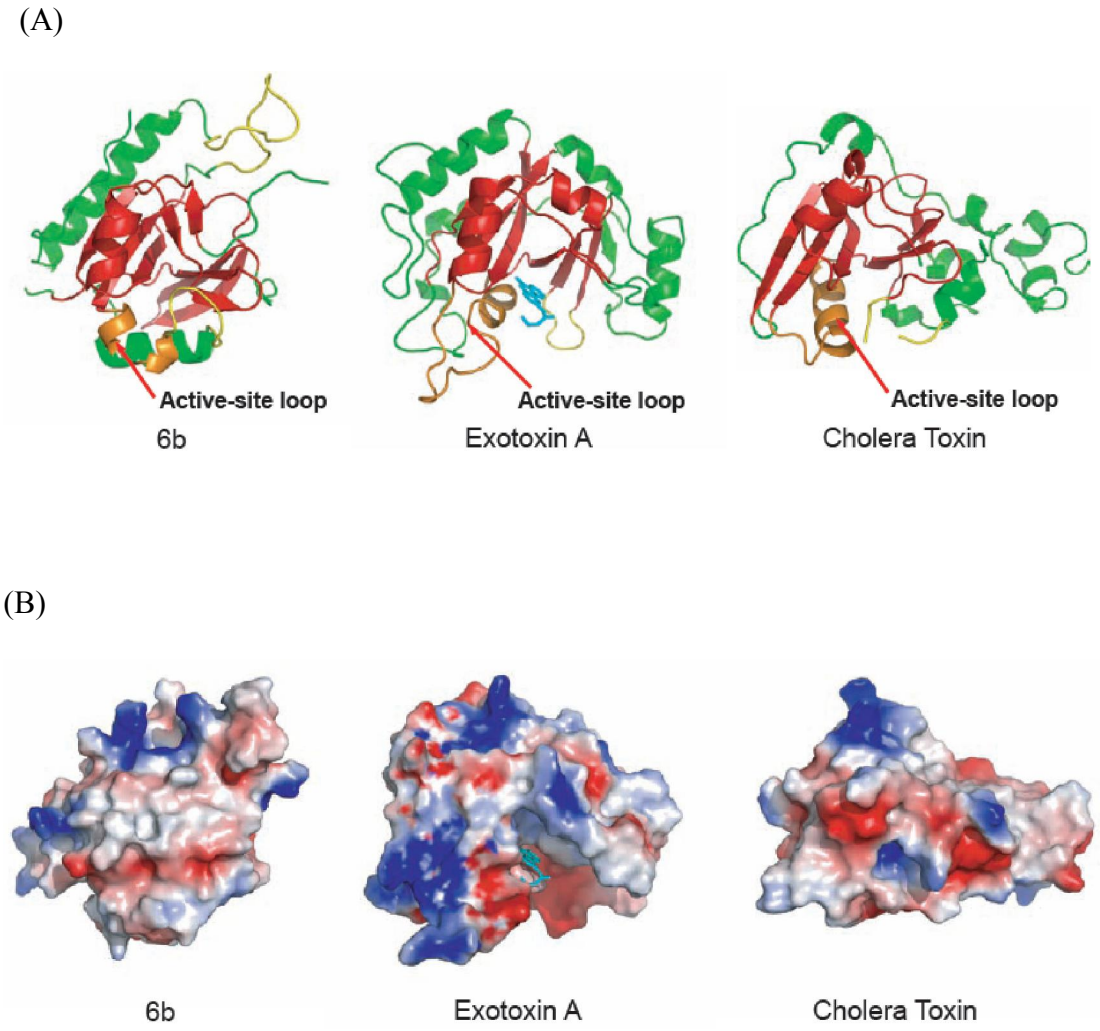

Fig. 10 AK6b is an ADP-ribosylating toxin.

(A): Ribbon representation of AK6b structure (left panel), Exotoxin A structure (middle panel) and Cholera toxin structure (right panel). The ADP-ribotransferase core domain is colored in red whereas the structural lid covered the active site is colored in orange. (B): Surface view of AK6b structure (left panel), Exotoxin A structure (middle panel) and Cholera toxin structure (right panel).

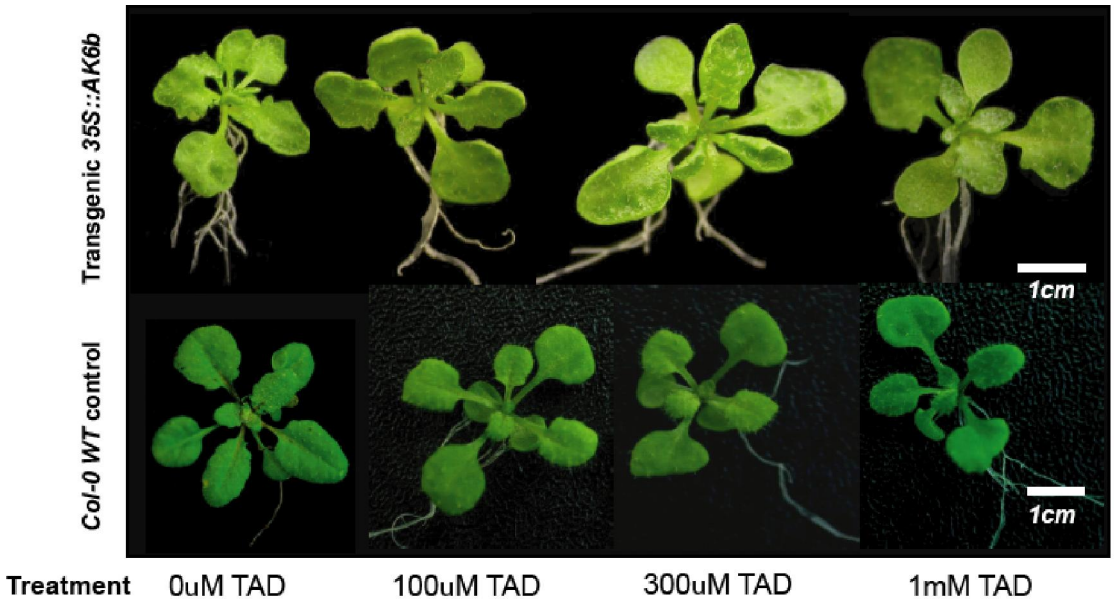

Fig. 11 Effects of TAD on morphology of *35S::AK6b* transgenic *Arabidopsis*. Plantlets of *Col-0* (Upper panel) and *35S::AK6b* transgenic seedlings (Down panel). Seeds were germinated on medium not supplemented with TAD (0μm) or supplemented with TAD (100μm, 300μm and 1000μm) and plants were grown for 23d. Bars: 1cm.

In the 6b structure, a long well ordered loop (residues 113-134) occludes the putative NAD^+ binding site, which must relocate to allow for substrate binding (Fig. 12A). This active-site loop may act as an arm to recognize ADP-ribose acceptor substrates. Consistent with the structural observation, *in vitro* ADP-ribosylation experiments showed that neither AK6b nor AB6b alone displays ADP-ribosylation activity (JY Yang, unpublished data). Interestingly, the conserved STS motif probably essential for NAD^+ binding in most ADP-ribosylating toxins is partially conserved at AK6b sequence (^{126}STNS^{129}). Similar to other ADP-ribosylating toxins, adjacent to the putative STS motif, one highly conserved aromatic residue amongst all 6b sequences (Tyr121) places its aromatic side chain into the putative NAD^+ binding pocket, suggesting that this aromatic residue may participate in NAD^+ binding (Fig. 12B).

In the 6b structure, a short loop (residues: 148-151) together with the connected

two anti-parallel β strands (β6 and β7) is aligned well with the ARTT motif conserved at both Exotoxin A and Cholera toxin structures (Fig. 12A). However, instead of conserved Glu-X-Glu (X, any amino acid) motif as catalytic residues, 6b has two invariable Tyr residues (Tyr153 and Tyr156) probably functioning as the putative catalytic residues (Fig. 12A). In our 6b structure, Tyr153 side chain points towards the NAD^+ binding pocket, whereas Tyr156 side chain points away from the NAD^+ binding pocket, suggesting Tyr 153 may play a primary catalytic role for ADP-ribosylation.

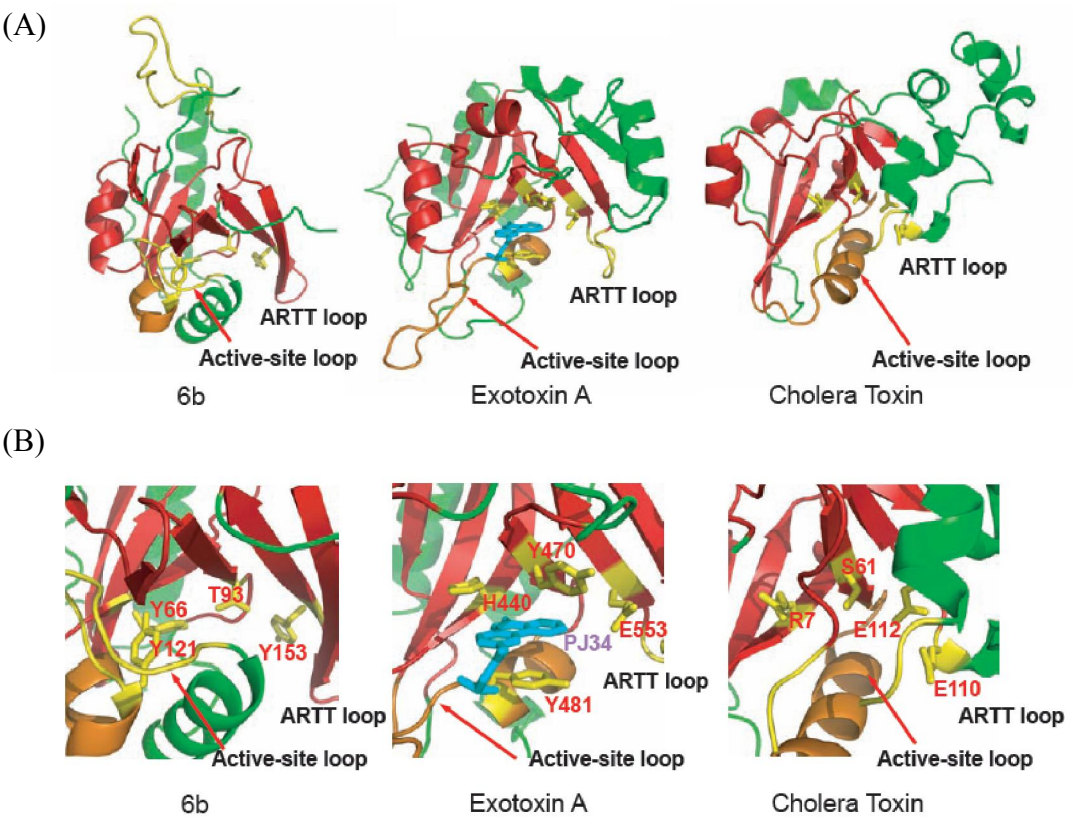

Fig. 12 Putative active site of AK6b.

(A):Overall view of putative active pockets of AK6b (left panel), Exotoxin A (middle panel) and Cholera toxin (right panel). The structural similar NAD^+ binding domain is colored in red and other subdomains are colored in green, whereas active-site loop is colored in orange. Active-site loop and ARTT loop are indicated and colored in yellow. (B): Detailed view of putative active pockets of AK6b (left panel), Exotoxin A (middle panel) and Cholera toxin (right panel). Catalytic residues involved in NAD^+ binding are indicated and colored in yellow.

3.5 Target binding loop

Strikingly, comparison of the crystal packing of AK6b and AB6b has revealed one conserved protein-protein interaction loop, which is unique to this family protein. In the AK6b structure, one bulky extra density was observed sandwiched between the C-terminal loop region (residues: 204-208) of 6b molecule 1 and one extended loop (residues: 40-55) of 6b molecule 2 (Fig. 13A). Due to the high-resolution of the AK6b structure, we were able to trace most of the NAD^+ molecules, including the ADP and the pyro-phosphate moieties. Interestingly, the same extended loop participating in crystal packing is also observed in the AB6b structure.

This conserved loop participating in crystal packing and protein-protein interaction in 6b crystal structures prompted us to test whether 6b protein self-associate and whether this loop plays a role in protein-protein interaction in vitro. In vitro pull-down assays showed that MBP-AK6b was able to pull down His-AK6b and His-AB6b (Fig. 13B). By contrast, MBP alone was not able to pull down His-AK6b or His-AB6b (Fig. 13B). Similarly, GST-AK6b was able to pull down His-AK6b and His-AB6b (Fig. 13B), whereas GST alone was not able to pull down His-AK6b or His-AB6b (Fig. 13B). In vitro pull-down assays further demonstrated that this extended loop (residues: 40-55) indeed participates in protein-protein interaction because MBP-AK6b (Δ40-55) was not able to pull down His-AK6b, whereas either GST-AK6b (Δ200-208) or MBP-AK6b (Δ164-184) was able to pull down His-AK6b (Fig. 13C).

To investigate whether this conserved loop also plays a general role for 6b to

interact with its target proteins, such as Arabidopsis Histone H3, we performed in vitro pull-down assay by immobilizing GST-AK6b on the GST beads or MBP-AK6b on the MBP beads and incubating His-SUMO-H3 with the bound GST-AK6b or MBP-AK6b protein. As expected, both GST-AK6b and MBP-AK6b were able to pull down His-SUMO-H3, whereas neither GST nor MBP alone was able to pull down His-SUMO-H3 (Fig. 13D). Similarly, in vitro pull-down assays further demonstrated that this extended loop (residues: 40-55) indeed plays a decisive role for H3 binding because MBP-AK6b (Δ40-55) was not able to pull down His-SUMO-H3, whereas both GST-AK6b (Δ200-208) and MBP-AK6b (Δ164-184) were able to pull down His-SUMO-H3 (Fig. 13E).

To investigate whether this extended loop (residues: 40-55) does play a significant role in vivo, we performed transgenic plant screen assay. Although, the severe morphological phenotypes displayed by overexpression of 35S::AK6b in *Col-0* Arabidopsis background, such as dwarf stem, leaf serration, have been largely reverted to those of the negative control *Col-0* line in the 35S::AK6b (Δ40-55) mutant overexpression lines (Fig. 13F), the protein expression levels of AK6b mutants in vivo, including this deletion mutant and those point mutants, are dramatically decreased beyond the detectable level (data not shown). These observation suggest that these critical residues and structural loop might also play important roles for protein stability in vivo, which are consistent with the similar observation of the effects of tumor growth on different plant species, such as *N. tabacum* and *K. daigremontiana* introduced by overexpression of 6b mutants based on sequence similarity analysis

(Helfer et al., 2002).

(A)

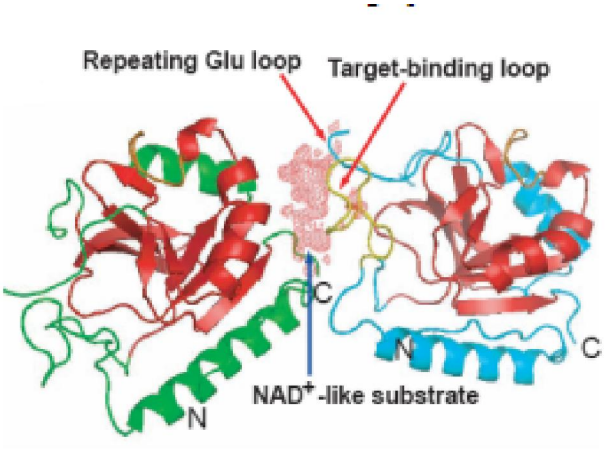

(B)

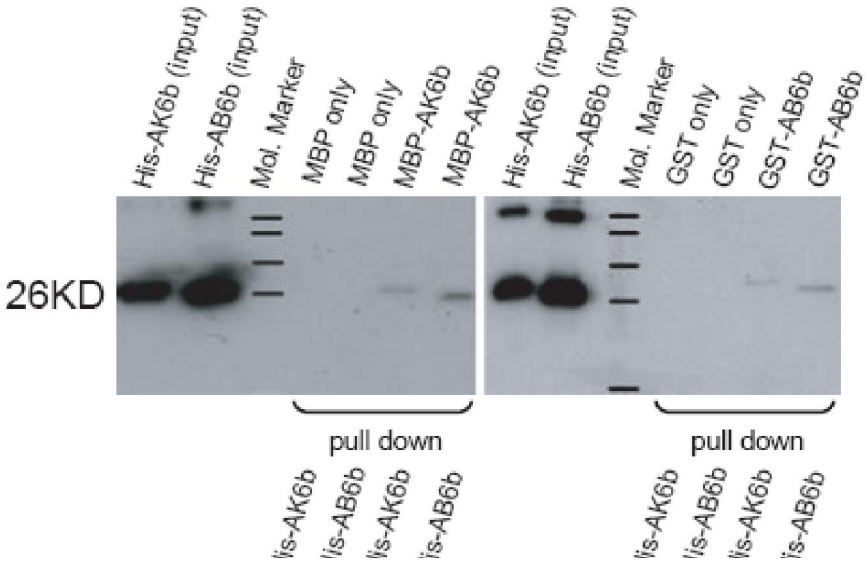

(C)

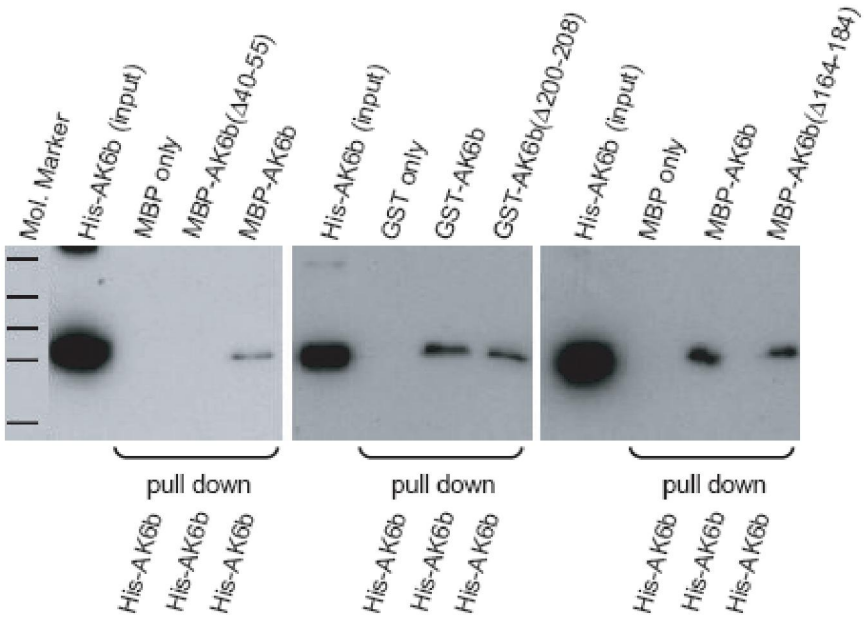

(D)

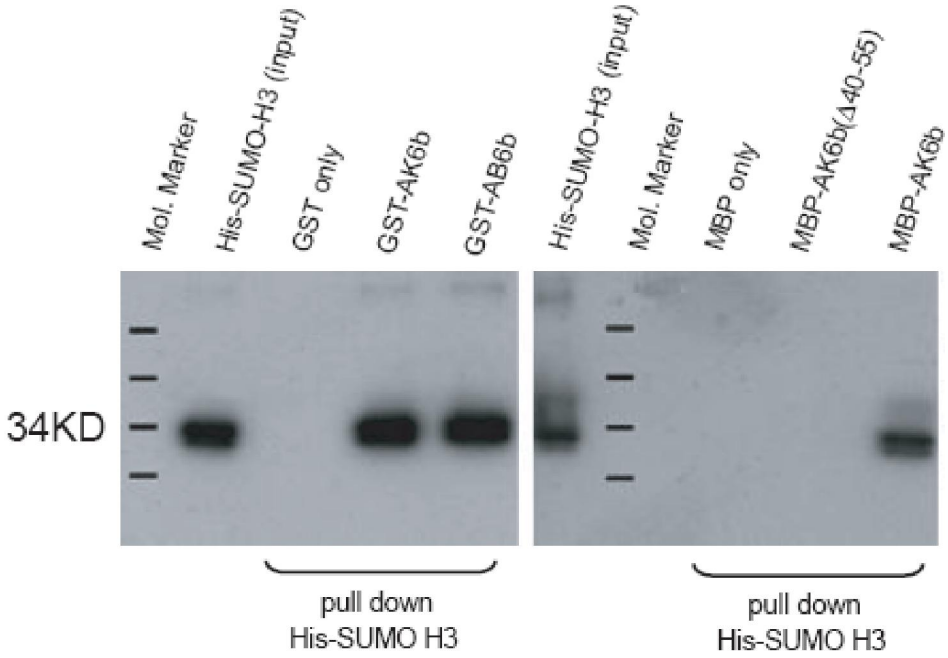
Mol. Marker
His-SUMO-H3 (input)
GST only
GST-AK6b
GST-AB6b
His-SUMO-H3 (input)
Mol. Marker
MBP only
MBP-AK6b(Δ40-55)
MBP-AK6b
34KD
pull down
His-SUMO H3
pull down
His-SUMO H3

(E)

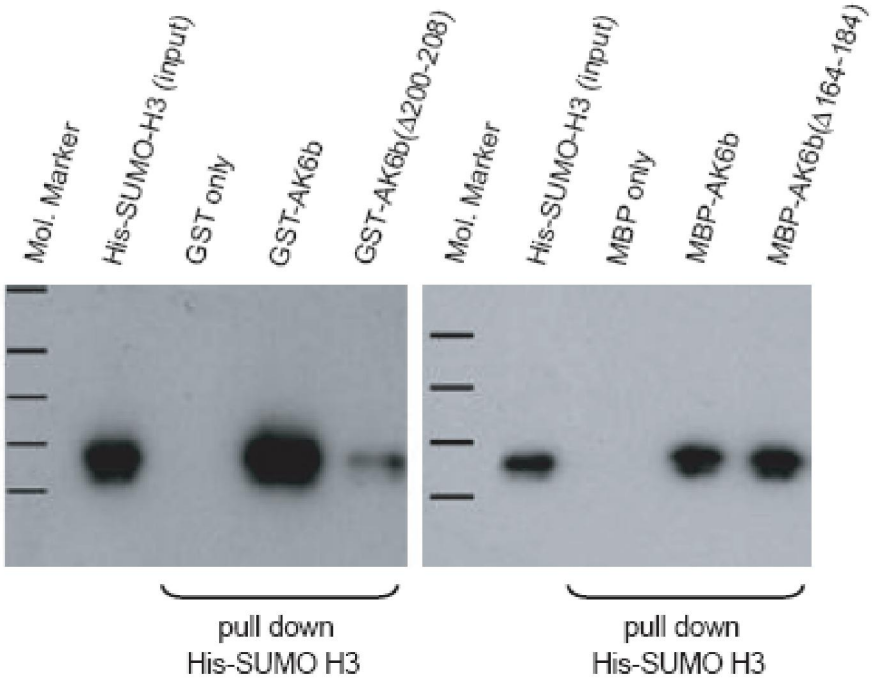
Mol. Marker
His-SUMO-H3 (input)
GST only
GST-AK6b
GST-AK6b(Δ200-208)
Mol. Marker
His-SUMO-H3 (input)
MBP only
MBP-AK6b
MBP-AK6b(Δ164-184)
pull down
His-SUMO H3
pull down
His-SUMO H3

(F)

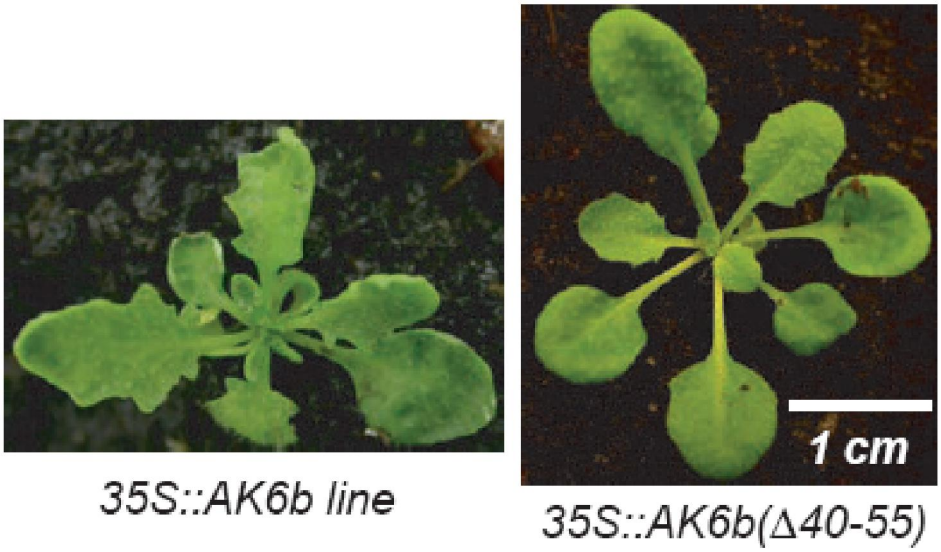

Fig. 13 Protein-protein interaction loop of AK6b.

(A): Crystal packing of AK6b (mediated by the putative NAD^+ molecule). The electron density of NAD^+ like substrate is colored in magenta, while the repeating Glu loop and the target-binding loop are indicated. (B, C): *In vitro* pull down assays of the self-interaction of AK6b and AB6b. (Upper panels) Coomassie brilliant blue G250 staining of the input of the GST-tagged or MBP-tagged bait proteins. (Down panels) The input and output of the 6His-tagged 6b prey proteins. Western blots were analyzed with monoclonal antibodies to poly-His. (D, E): *In vitro* pull down assays of *Arabidopsis* Histone H3 by AK6b and its mutant derivations. The input of the GST-tagged or MBP-tagged bait proteins are same with (B). (Down panels) The input and output of the 6His-SUMO-tagged prey proteins H3. Western blots were analyzed with monoclonal antibodies to poly-His. (F): Morphological phenotype of transgenic plants expressing *35S::AK6b* (left) and *Δ40-55* mutant (right). Photographs were taken for 4-wk-old seedlings. Bars: 1cm.

3.6 6b interferes with miRNAs pathways in *Arabidopsis*

MicroRNAs (miRNAs) and short interfering RNAs (siRNAs) function as sequence-specific guides to silence genes, transposons and viruses, and to modify the chromatin structure. miRNAs are involved in the control of various plant developmental processes, including leaf morphogenesis (Palatnik et al, 2003), floral development (Chen, 2004), root development (Guo et al, 2005), vascular development

(Kim et al, 2005) and the transition from vegetative to reproductive phases (Lauter et al, 2005). Many miRNAs regulate plant development by delimiting the regions of accumulation of transcripts encoding transcription factors that function in development (Kidner & Martienssen, 2005). This explains the pleiotropic developmental phenotypes of plant mutants defective in miRNA accumulation, such as dicer-like1 (dcl1), hua enhancer 1 (hen1), hyponastic leaves 1 (hyl1) and argonaute 1 (ago1) (Park et al, 2002; Boutet et al, 2003; Vaucheret et al, 2004; Vazquez et al, 2004). The maturation of both types of small RNA is catalyzed by double-stranded RNA (dsRNA)-specific RNaseIII-like enzymes called DICER-LIKE (Park et al, 2002). DCL1 processes miRNA precursors (Park et al, 2002; Kurihara & Watanabe, 2004) with two other proteins HEN1 (Boutet et al, 2003; Yu et al, 2005) and HYL1 (Han et al, 2004). The short dsRNAs produced by DCL activity are assembled into effector complexes and they guide sequence-specific degradation of complementary target messenger RNAs, translational repression of target mRNAs or condensation of heterochromatin (Meister & Tuschl, 2004). ARGONAUTE (AGO) proteins are components of these silencing effector complexes.

Carefully comparison of the morphological phenotypes of *35S::AK6b* overexpression line with *ago1-27* and *se-1* mutant lines showed that *35S::AK6b* overexpression line partially phenocopied these miRNA deficient mutant lines, which have strongly serrated leaves (Fig. 14). This observation prompted us to test whether *6b* interferes with miRNA pathway in *Arabidopsis* by using northern blotting to investigate the expression levels of several miRNAs (miR162, miR164, miR165/166

and miR319) involved in leaf development and their target mRNAs. Along with the severe morphological phenotype accompanying with the overexpression of *35S::AK6b* in *Arabidopsis*, miR162, miR164 and miR319 were significantly decreased, whereas miR165/166 was slightly decreased (Fig. 15). On the other hand, the Real-time PCR results showed that the mRNA targets of these miRNAs accumulated to a high level inversely-correlated to the low expression level of the individual miRNAs (Fig. 16). Notably, the molecular miRNA deficient phenotypes of *35S::AK6b* overexpression line and *se-1* mutant line only partially overlapped. For example, the expression level of miR319 was significantly decreased in *35S::AK6b* overexpression line instead of the *se-1* mutant line (Fig. 15). By contrast, the expression level of miR165/166 was significantly decreased in *se-1* mutant line instead of *35S::AK6b* overexpression line (Fig. 15). Similarly, the accumulation of their target mRNAs, such as *TCP4* (miR319 target) and *REV* (miR165/166 target), in *35S::AK6b* overexpression line and *se-1* mutant line are inversely-correlated to the individual miRNA expression level (Fig. 16).

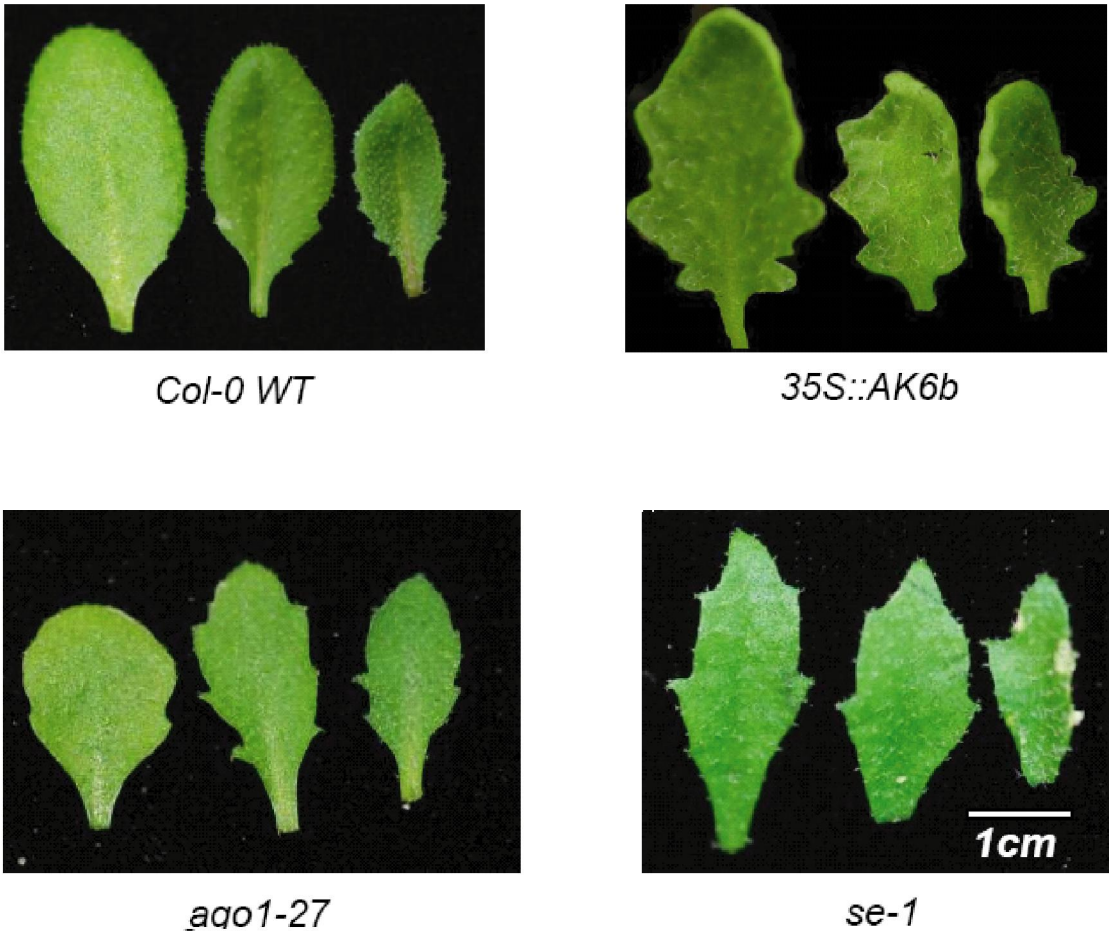

Fig. 14 Expression of miRNA in *AK6b* transgenic plants.

Comparison of the morphological phenotype between 3*5S::AK6b*, *ago1-27* and *se-1* plants. Photographs were taken for the 2nd, 3rd and 4th true leaves of the 4-wk-old seedlings. Bars: 4mm.

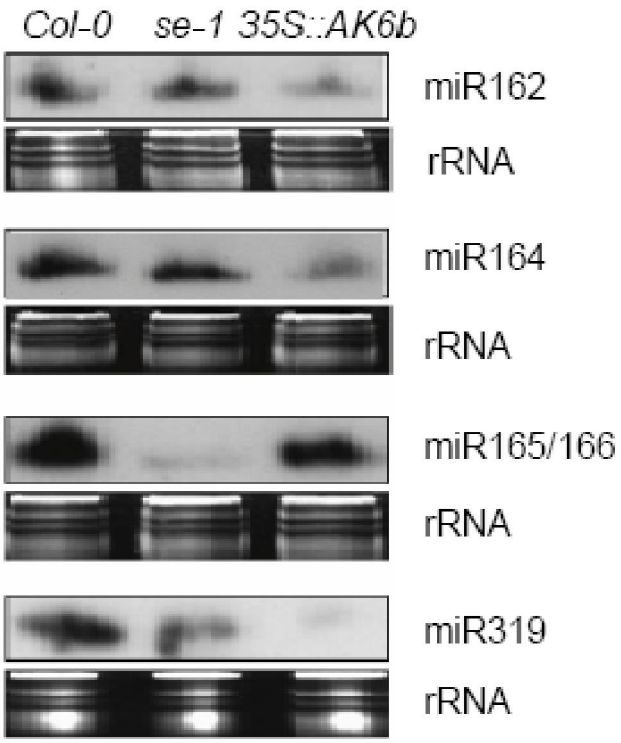

Fig. 15 Northern blot results showed the accumulation of small RNAs in WT (*Col-0*), *se-1* and *35S::AK6b* plants.
rRNAs were used as a loading control. Each lane contained 12μg RNA.

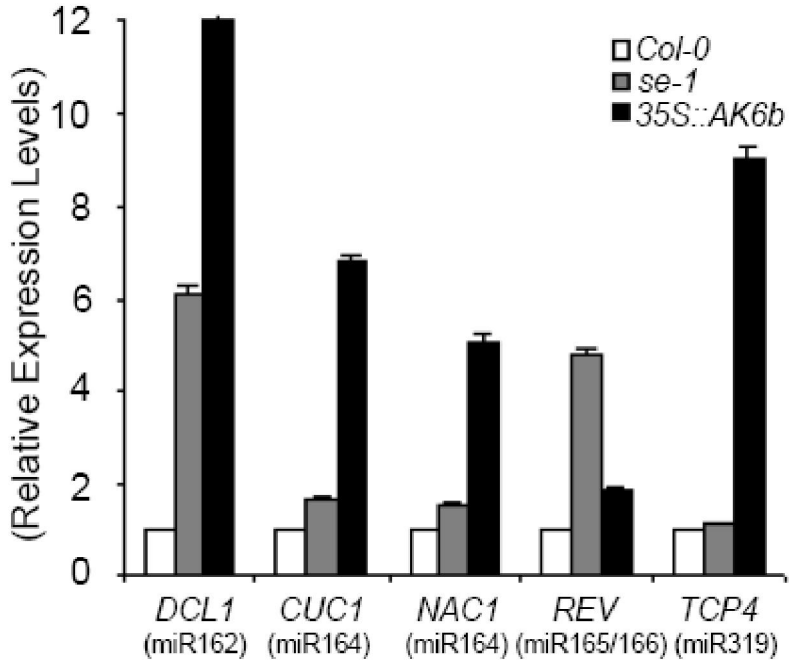

Fig. 16 Real-time RT-PCR results showed the accumulation of the target mRNAs in WT (*Col-0*), *se-1* and *35S::AK6b* plants.
Quantifications of each cDNA sample were made in triplicate, and the consistent results from at least two separately prepared RNA samples were used.

3.7 6b targeting Arabidopsis AGO1 and SE *in vitro* and *in vivo*

The partially overlapping miRNA deficient phenotypes amongst *35S::AK6b* overexpression line, *se-1* mutant line and *ago1-27* mutant line prompted us to test the possible direct interactions between AK6b and SE or AGO1. We performed *in vitro* pull-down assays using various purified protein fragments to examine whether the AK6b-AGO1 or AK6b-SE interaction is direct and attempt to map the interaction domains. We systematically generated 6 truncated AGO1 mutants from N-terminus to C-terminus. *In vitro* pull-down assays showed that AGO1 NT fragment (residues 185-371) is the primary interaction domain targeted by AK6b (Fig. 17A). This fragment corresponds to the entrance channel for the small RNA and its target mRNA (Fig. 17B).

Similarly, we generated three truncated SE fragments from N-terminus to C-terminus systematically. *In vitro* pull-down assay showed that both SE-NT fragment (residues 194-240) and SE-Mid fragment (residues 241-469) are the interaction domains targeted by AK6b (Fig. 18). To investigate whether this extended loop (residues: 40-55) also plays a role in SE binding, we performed *in vitro* pull-down assay. Our assay confirmed that this extended loop (residues: 40-55) indeed plays a decisive role for SE binding because MBP-AK6b (Δ40-55) was not able to pull down His-SE, whereas both GST-AK6b (Δ200-208) and MBP-AK6b (Δ164-184) were able to pull down His-SE (Fig. 19).

(A)

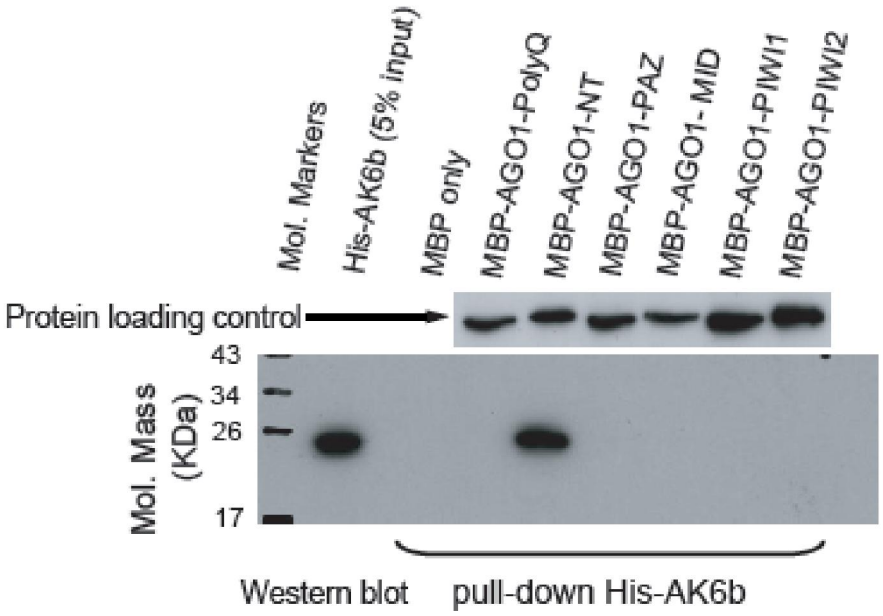

(B)

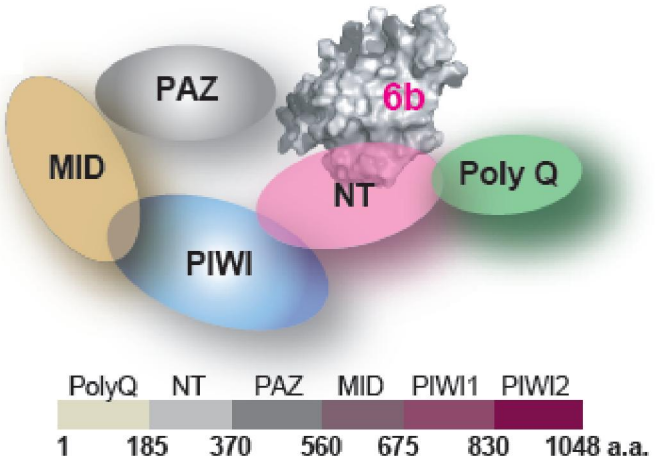

Fig. 17 Interaction of AK6b and AGO1 *in vitro* and *in vivo*.
(A): *In vitro* pull-down assays of His-AK6b interaction with MBP-AGO1 fragments. MBP-AGO1 fragments were immobilized on the MBP beads and individually incubated with His-AK6b. Bound MBP-AGO1 fragments were retrieved and the association of AK6b was monitored by Western blots using monoclonal antibodies against poly-His. (Upper panel) Western blot results for the input of MBP-AGO1 fragments using ttAgo1 polyclonal antibody. (Down panel) The input and output of pulled-down His-AK6b. (B): A cartoon showing binding of AK6b to one surface of the PAZ-containing module of AGO1 which harbors small RNA and its target mRNA binding groove. Individual predicted domains were indicated on the cartoon figure. A schematic diagram showing the domain borders in *Arabidopsis* AGO1 was given underneath.

(A)

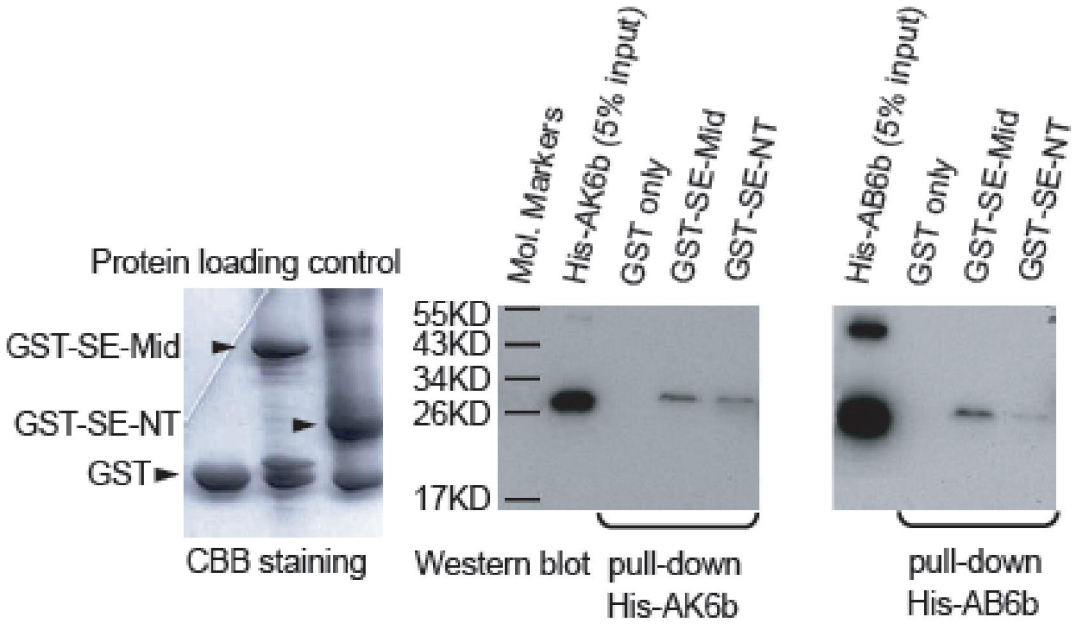

(B)

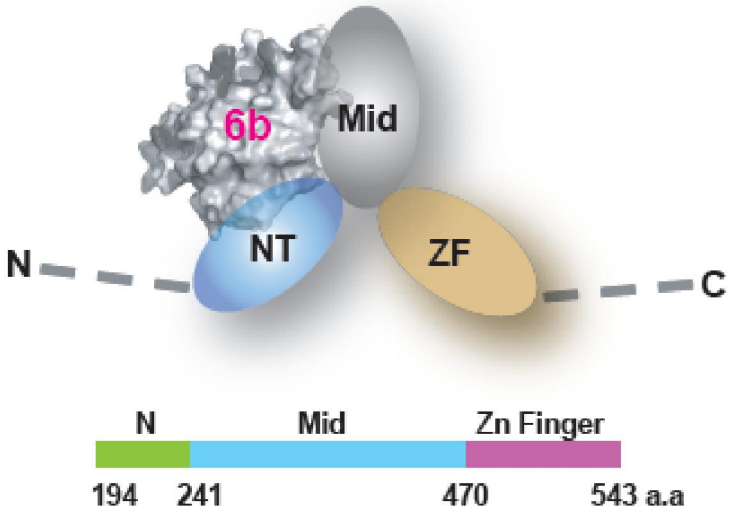

Fig. 18 Interaction of AK6b and SE *in vitro* and *in vivo*.

(A): *In vitro* pull-down assays of SE fragments and 6b proteins. GST-SE-Mid and GST-SE-NT were individually immobilized on the GST beads and His-AK6b or His-AB6b was incubated with bound SE fragments. Western blots were analyzed with monoclonal antibodies against Poly-His. (Upper panel) Coomassie brilliant blue G250 staining of the input of SE fragments. (Down panel) The input and output of pulled-down His-AK6b or His-AB6b. (B): A cartoon showing binding of AK6b to one surface of the SE core domain, which probably harbors the protein-protein interaction platform. Individual predicted domains were indicated on the cartoon figure. A schematic diagram showing the domain borders in *Arabidopsis* SE core domain was given underneath.

(A)

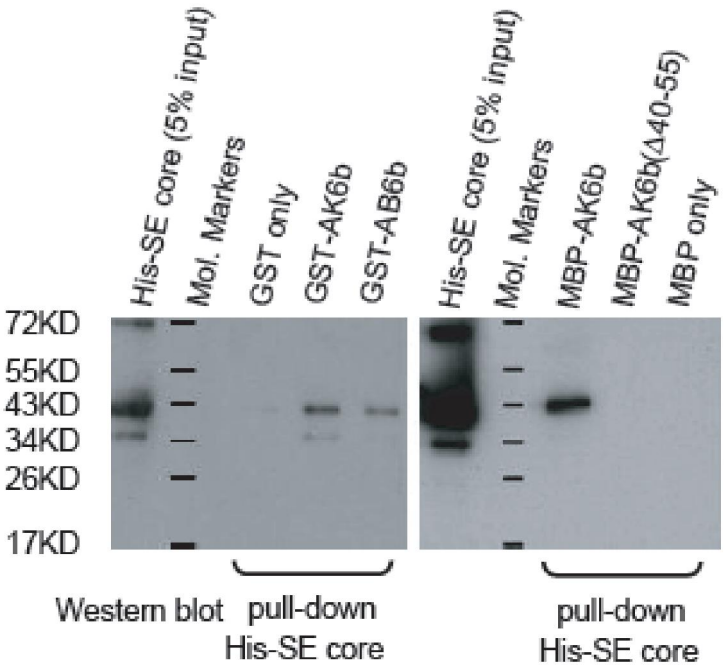

(B)

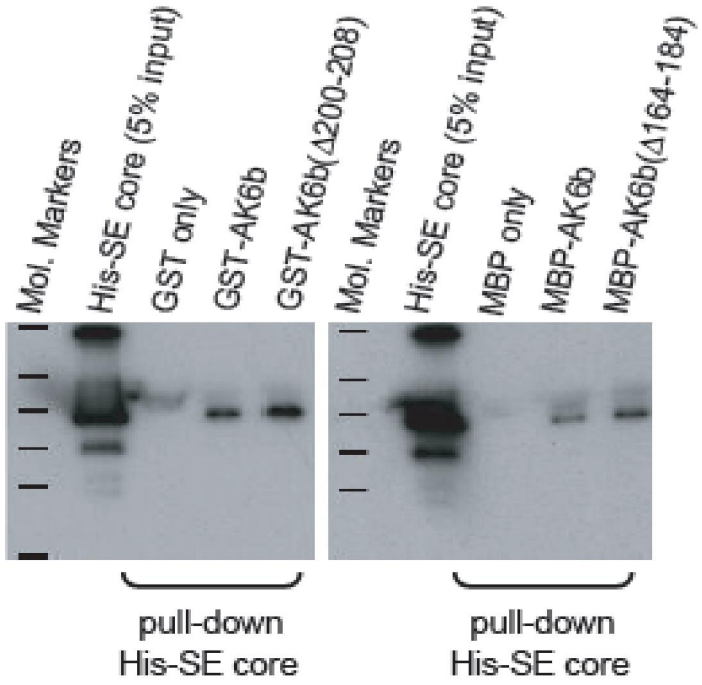

Fig. 19 *In vitro* pull down assays of 6b proteins with His-SE core fragment.

(Upper panels) Coomassie brilliant blue G250 staining of the input of the GST-tagged or MBP-tagged bait proteins. (Down panels) The input and output of the prey protein His-SE core fragment. Western blots were analyzed with polyclonal antibodies to SE-core.

(A)

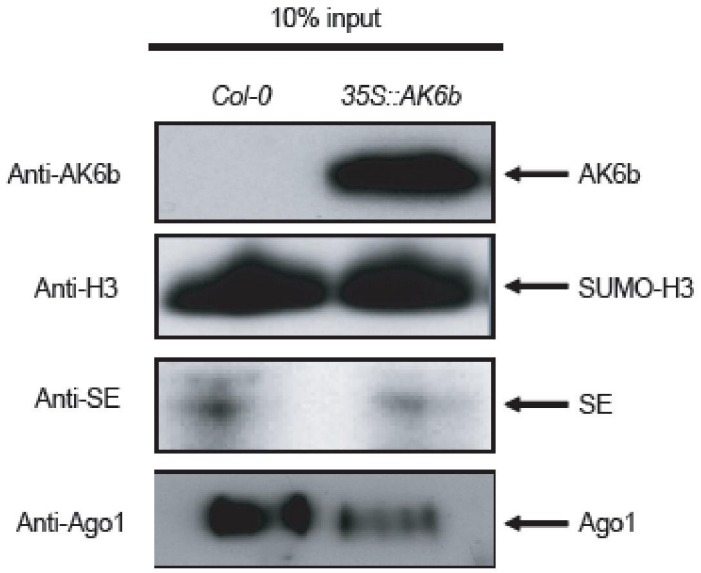

(B)

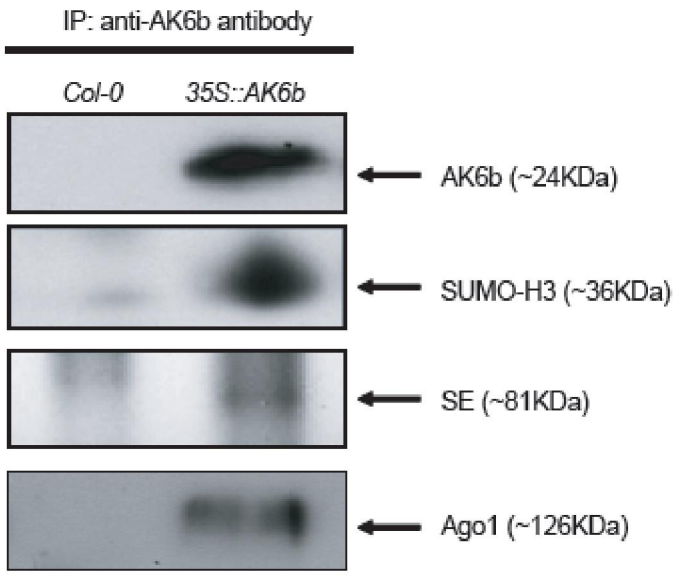

Fig. 20 Interaction of AK6b and SE fragments in *Arabidopsis* plants *in vivo*.

Two-week old seedlings expressing *35S::AK6b* were treated overnight with 50 μM MG132. Total protein extracts were immunoprecipitated (IP) with polyclonal antibody to AK6b. Western blots were analyzed with an AK6b polyclonal antibody to detect AK6b (top panel), an H3 polyclonal antibody to detect *Arabidopsis* Histone H3 (the 2nd panel), SE polyclonal antibody to detect co-immunoprecipitated SE (the 3rd panel) and ttAgo1 polyclonal antibody to detect co-immunoprecipitated Ago1 (bottom panel).

To investigate whether 6b interacts with SE *in vivo*, we performed co-immunoprecipitation (Co-IP) experiments using extracts prepared from 3*5S::AK6b* overexpression plants. We found that the SE antibody indeed detected a band in the immuno-complex pulled down by AK6b antibody (Fig. 20). At this moment, we are unable to detect the AGO1 band from the immuno-complex pulled down by AK6b antibody probably due to the low quality of the bacterial AGO antibody we have in hand. Work is in progress to generate the *35S::AK6b* overexpression lines in the Flag-AGO1 background to repeat this experiment.

Finally, in order to further confirm the direct interaction of AK6b with AGO1 and SE, colocalization assay was performed. Fluorescent proteins were fused to the C-terminus of AK6b, AGO1 and SE to generate cyan fluorescent protein [CFP]: AK6b, yellow fluorescent protein [YFP]: AGO1 and YFP: SE. Firstly, large amount of plasmid, about 60μg each contruct, was prepared for particle bombardment (Fig. 21). After bombardment, the fluorescent signals were analyzed by confocal. Fig. 22 shows that AGO1 was distributed widely in the cytoplasm and the nucleus in a manner similar to YFP, whereas AK6b and SE were localized preferentially in the nucleus. When AGO1 or SE was coexpressed with AK6b, the proteins colocalized in the nucleus.

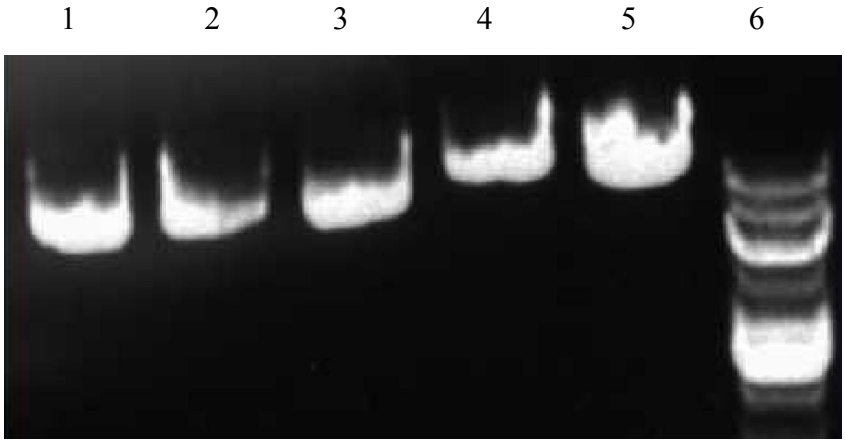

Fig. 21 Plasmids used for bombardment into onion epidermal cells.

Lane 1-5: pBA002-YFP, pBA002-CFP, pBA002-AK6b-CFP, pBA002-Ago1-YFP and pBA002-SE-YFP; Lane 6: 1Kb marker.

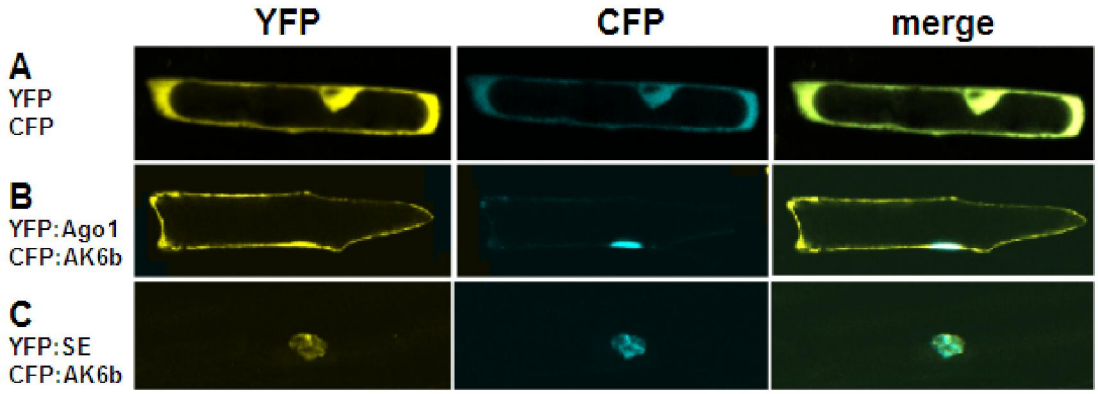

Fig. 22 AK6b Colocalizes with Ago1 or SE in the Nucleus.

Epidermal onion cells were transformed transiently with vectors expressing the following fluorescent proteins: YFP+CFP (A), YFP: Ago1+CFP: AK6b (B) and YFP: SE +CFP: AK6b (C). Signal from YFP, CFP, and the merge of both signals are shown in the left, middle, and right columns, respectively. Bars=50μm.

Chapter 4 Discussion

4.1 6b belongs to a novel toxin family

Although having limited sequence homology, ADP-ribosylating toxins share a common core structures for NAD^+ binding. However, the toxins can be divided into two groups with the DT group represented by Exotoxin A and CT group represented by Cholera toxin. The completely different sets of catalytic residues within the active site used by these two different toxin groups (DT *vs.* CT) strongly suggest that the mechanisms of substrate recognition could be different (Deng and Barbieri, 2008).

In Exotoxin A structure, the active site is composed of characteristic residues Glu553, His440, Tyr481 and Tyr470 (Fig. 12, middle panel). Glu553 forms a hydrogen bond with the 2'OH of N-ribose of NAD^+ and orientates the dinucleotide substrate for nucleophilic attack, whereas His440, Tyr481 and Tyr470 stabilize the bound NAD^+ substrate (Fig. 12, middle panel). Moreover, comparison of the structures of apo-Exotoxin A and that of the EF2 complex demonstrated that the contact surface between ExoA and its EF2 target is rather small and the conformational changes is marginal on NAD^+ binding or EF2 binding or during the substrate catalysis process (Jorgensen et al., 2005; 2008).

By contrast, in Cholera toxin structure, the active site is composed of characteristic residues Arg7, Ser61, Glu110, and Glu112, which is occluded by the active-site loop (residues 47 to 56) (Fig. 12, right panel). Upon binding to its partner protein, such as ARF6-GTP, this loop swings out of the active site to exposes residues

for substrate binding and catalysis (Lobet et al., 1991 and Cieplak et al., 1995; Akker et al., 1996; O'Neal et al., 2004).

6b protein contains a conserved central module resembling the overall structural similarity to the NAD^+ binding pockets of all the ADP-ribosylating toxins discovered so far, although there is no apparent sequence similarity between 6b and ADP-ribosylating toxins. Moreover, 6b represents a novel family of ADP-ribosylating toxins (Fig. 12 left panel), which contains another completely different set of catalytic residues within the putative NAD^+ binding pocket (Fig. 12B, left panel). The well conserved Glu (Exotoxin A and Cholera toxin) or His/Arg (Exotoxin A/Cholera toxin) is not available within the 6b active-site pocket. Instead, highly conserved Tyr66 and Tyr153 residues are employed to probably replace the functions displayed by Glu and His/Arg residues, respectively. In addition, the critical highly conserved Thr93 probably plays the same functional role as Tyr470 at Exotoxin A or Ser61 at Cholera toxin by forming hydrogen bonds with the catalytic Tyr153 residue to facilitate ADP-ribosylation (Fig. 12, left panel). Furthermore, similar to Cholera toxin, the active-site pocket of 6b is occluded by the active-site loop (residues 113-134) (Fig. 12A, left panel). Therefore, significant conformational changes are required to expose this active-site pocket to allow for NAD^+ access. Consistent with this structural observation, 6b does not display any ADP-ribosylation function *in vitro* on any target proteins discovered so far (data not shown). Therefore, *Arabidopsis* partner proteins are probably recruited by 6b and presumably trigger the conformational change *in vivo*.

4.2 6b directly targets miRNA machineries

RNA silencing is a conserved eukaryotic post transcriptional gene regulation mechanism that targets and degrades aberrant endogenous or exogenous RNA molecules. (Sontheimer, 2005) This phenomenon was first discovered in plants, whereby the introduction of additional copy of the flower pigmentation chalcone synthase (CHS) gene resulted in suppression of both the introduced transgene and the endogenous RNA. Transgenic plants showed flowers with either reduced pigmentation or complete absence of pigmentation (Napoli, 1990). These observations were described as cosuppression or posttranscriptional gene silencing (PTGS) in plants.

Inaddition to plants, RNA silencing was also manifested in fungi *Neurospora crassa*. Introduction of homologous RNA sequences has resulted in sequence-specific RNA degradation or 'quelling' of the endogenous gene (Romano, 1992). Consistently, the same mechanism has also been identified in animal *Caenorhabditis elegans.* Endogenous RNA underwent degradation after the introduction of the sense and antisense RNA (Guo and Kemphues, 1995). In 1998, the term RNA interference (RNAi) was introduced when a major breakthrough came with the observation that injection of the double-stranded RNA in *C.elegans* has caused strong degradation of the endogenous mRNA. This suppressing effect has been demonstrated to be more potent than injection of either strand individually (Fire et al., 1998). These observations provide evidence that RNA silencing is conserved across kingdoms. The biochemistry of RNA silencing mechanism has been well studied using *Drosophila*

embryo extracts. The process involves the endonucleolytic cleavage of the longer doublestrand RNA molecules into small interfering RNA (siRNA) species by an RNase-III-type Dicer-like enzyme (Schnettler, 2008). These small RNA molecules are 21-26 bp in size which contain 2 nt 3' overhangs and 5' phosphorylated termini. The siRNA duplexes are then incorporated into the RNA-induced silencing complex (RISC) and trigger sequence specific identification of the RNA targets. Enzymatic activity of members of the Argonaute (AGO) protein family allows the programmed RISC to slice the complementary mRNAs (Fagard, 2000; Hammond et al., 2000). As a consequence, it leads to the knock down of the targeted gene and results in loss of functions displayed by the specific protein. This mechanism has been identified to play a major key role in antiviral defense (Lakatos, 2006). Beisdes siRNA, there are other short regulatory RNAs in the RNA silecning machinery known as microRNAs (miRNAs). miRNAs are the host encoded endogenous small RNA molecules which are involved in post-transcriptional regulation. miRNA targets cellular transcripts with small stretch of homology by either guiding their degradation or inhibiting their translation (Bartel, 2004). The process involves the synthesis of the Pri-mRNA from the MIR genes in the nucleus and it is subsequently recognised and cleaved by Drosha protein into precursor PremiRNA. They are then exported out into the cytoplasm with the help of Exportin-5 and processed by the Dicer enzyme into mature miRNA/miRNA duplexes (Kim, 2004; Yi et al., 2003). miRNA strand is then incorporated into a RISC-like complex and the miRNA strand degraded (Parker et al., 2005). Mature miRNA in animal will induce translational repression of the targets

while in plants miRNA, the target mRNA are more likely to undergo mRNA cleavage by AGO1 enzyme (Bartel, 2004; Baumberger and Baulcombe, 2005). This mechanism has been known to be crucial in controlling gene expression during developmental process. In plants, RNA silencing is an important antiviral defense and it is initiated by highlystructured viral RNAs, dsRNA replication intermediates of plant viruses, cytoplasmically replicating viruses or dsRNA produce by plant RNA dependent RNA polymerase (RDR) action (RDR1 or RDR6) (Hemmes, 2007). Processing of viral specific dsRNAs subsequently results in the accumulation of viral siRNAs that triggers the RNA silencing process. Interestingly, in addition to the 21nt siRNA, a second class of larger siRNAs (24-26nt) were also found in plant antiviral mechanism that seem to be involved in systemic signaling and are proposed to travel to different plant organs in advance of the invading virus (Hemmes, 2007; Mlotshwa et al., 2002).

Interference with RNA silencing by viral suppressors represents an anti-host defense response by viral pathogens (reviewed by Yang and Yuan, 2009). The Ti plasmid (T-DNA) can be considered to be functionally related to DNA virus. The observation that *35S::AK6b* overexpression in the *Col-0* background displaying similar morphological phenotype as that of *35S::FNY2b* plants raises the question whether protein 6b functions as a RNA silencing suppressor (Zhang, et al., 2006). The partially overlapping morphological and molecular phenotypes between *35S::AK6b* overexpression line and *ago1-27* and *se-1* mutant lines further suggest that 6b probably interferes with miRNA pathways (Fig. 14). Our results show that AK6b

probably executes its suppressor function by direct targeting SE and AGO1, two key components of miRNA machineries in *Arabidopsis* (Fig. 17, 18). We have also mapped the primary targeting region on AGO1 to the N-terminal domain adjacent to the RNA entrance groove and the primary interacting regions on SE to the protein-protein interaction platform including the N-terminal domain and the Mid domain (Fig. 17, 18).

The specific 6b/SE and 6b/AGO1 interactions probably suggest that not only RISC/AGO1 but also DCL1-SE-HYL1 are essential protein complexes that participate in virus-induced gene silencing (VIGS) to defend against offending viruses. Compared to other viral suppressors primarily targeting on AGO1, such as CMV2b and P0 (Zhang et al., 2006; Baumberger et al., 2007; Bortolamiol et al., 2007), 6b protein targets a wide arrange of host protein residing inside the nucleus (Kitakura et al., 2002; Terakura et al., 2007; Kitakura et al., 2008). The ADP-ribotransferase fold displayed by 6b structure probably enables 6b to function as an ADP-ribosylating toxin to target many host proteins with apparently completely different functions, although we are unable to detect ADP-ribosylation activity of 6b in vitro so far.

Interestingly, although both 6b and CMV2b target AGO1 to interfere with miRNA pathway in plants, the primary target of 6b seems to be SE because the miRNA expression levels at the 35S::AK6b overexpression lines are dramatically decreased (Fig.15)

4.3 Potential roles of 6b on plant gene regulation and cell growth

6b proteins interact with many different proteins involved in expression of plant genes related to cell proliferation with various hypotheses proposed to explain the effects of 6b on the growth of plant cells. The repeating Glu residues loop (residues 164-184) was reported to interact with NtSIP1, which contains the tri-helix motif (Kitakura et al., 2002); and NtSIP2, which is entirely homologous to the TNP1 protein (Kitakura et al., 2008). However, 6bΔA mutant protein (lacking the repeating Glu residues loop: 164-184) retains the ability to interact with *Arabidopsis* histone H3, SE and AGO1 (Terakura et al., 2007 and our data). It seems that there are two groups of proteins interacting with 6b: one group targeting this acidic loop and the other group targeting other structural elements. The acidic loop (residues: 164-184), which may serve as a structural scaffold for protein-protein or protein-nucleic acid interaction, is disordered in both AK6b and AB6b structures. By contrast, we have identified one well-ordered loop (residues 40-55), which serves as a structural scaffold for *Arabidopsis* histone H3, AGO1 and SE binding (Fig. 13, Fig. 17, 18 and 19).

The fact that 6b protein targets to a wide arrange of diversified host proteins in plants suggests that the phenotypes generated by the expression of 6b might depend on the types of 6b-interacting proteins. On one hand, 6b might function as a transcriptional coactivator/mediator by interacting with the proteins involved in the transcription machinery mediated by the repeating acidic Glu residues loop; one the other hand, 6b might function as a ADP-ribosylating toxin by targeting key components in the miRNA processing /silencing machinery with the well ordered

extended loop (residues: 40-55) (Fig. 23). The ectopic expression of a number of genes, such as class I KNOX, CUC and cell cycle-related genes, caused by 6b expression probably depends on the general ADP-ribosylation activity of 6b. Since the covalent modifications to host targets catalyzed by ADP-ribosylation often result in an inactivation of the targets, therefore the transgenic *Arabidopsis* plants that carried the 6b gene exhibiting various developmental abnormalities, including leaf curling, serration and dwarfism are probably due to the ADP-ribosylation activity. ADP-ribosylation modification of host target proteins by 6b may result in an inactivation of the target proteins, which eventually changes cell physiology and even produces the tumors. Consistent with this hypothesis, the mutations on the conserved ADP-ribosylation catalytic residues Tyr66 or Thr93 lead to a loss of 6b oncogenicity (Helfer, et al., 2002). Moreover, the abnormal growth of calli induced by 6b is probably also dependent on the ADP-ribosylation activity because the 6bΔC mutant protein (lacking residues 164-208), which disrupts the overall ADP-ribosylation fold, did not trigger any abnormal growth of calli (Kitakura et al., 2002; Terakura et al., 2007).

Although *6b* gene might only play a minor role in crown gall formation, it could play a much more important role in tumorigenicity in certain host species (Garfinkel et al., 1981; Joos et al., 1983; Hooykaas et al., 1988; Tinland et al., 1989; Tinland et al., 1992). These observations are also consistent with our structural evidence that 6b protein is a novel ADP-ribosylating toxin, which has certain host target specificity. A major challenge in the future is to identify and incorporate the host partner protein of

6b into account. The structure determination of the 6b-partner complex will eventually to unveil the molecular mechanism of 6b in details.

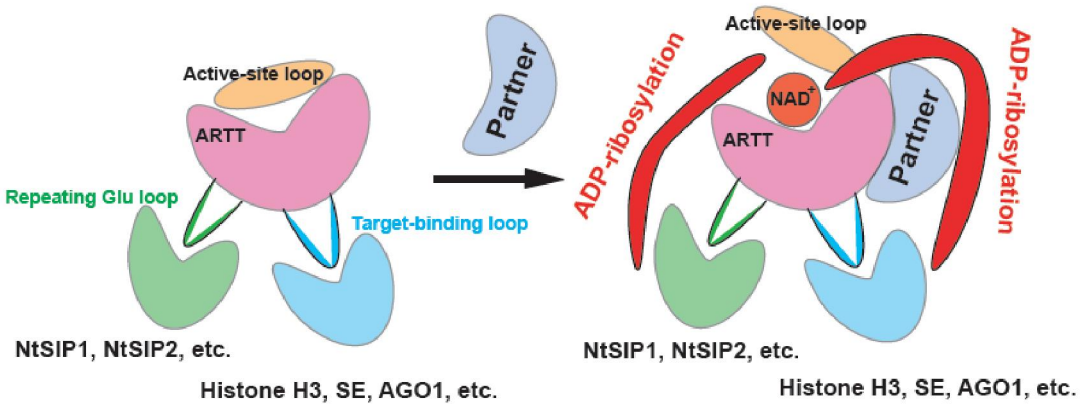

Fig. 23 A hypothetical working model describing the roles of 6b on plant gene regulation.

6b is a novel ADP-ribosylating toxin with the active NAD^+ binding pocket closed by a structural lid. Upon the binding of host partner protein, the lid will be moved away from the active pocket to let the pocket accessible for NAD^+ binding. There are two different extended loops at the surface of 6b, which are the targets for interacting protein. One family of host proteins, such as NtSIP1 and NtSIP2, bind to the repeating Glu residue loop (residues: 164-184), whereas the other family host proteins, such as H3, AGO1 and SE, bind to the other loop (residues: 40-55). Upon substrate proteins binding, 6b probably inactivates these host target proteins by ADP-ribosylation modification. Such approaches enable 6b to affect many proteins involved in plant cell proliferation regulation.

References

Bartel, D.P. (2004). MicroRNAs: Genomics, Biogenesis, Mechanism, and Function. Cell *116*, 281-297.

Baumberger, N., and Baulcombe, D.C. (2005). Arabidopsis ARGONAUTE1 is an RNA Slicer that selectively recruits rnicroRNAs and short interfering RNAs. Proc Natl Acad Sci U S A *102*, 11928-11933.

Baumberger, N., Tsai, C.H., Lie, M., Havecker, E., and Baulcombe, D.C. (2007). The Polerovirus silencing suppressor P0 targets Argonaute proteins for degradation. Curr. Biol. *17*, 1609-1614.

Bonnard, G., Tinland, B., Paulus, F., Szeqedi, E., and Otten, L. (1989). Nucleotide sequence, evolutionary origin and biological role of a rearranged cytokinin gene isolated from a wide host range biotype III Agrobacterium strain. Mol. Gen. Genet. *216*, 428-438.

Bortolamiol, D., Pazhouhandeh, M., Marrocco, K., Genschik, P., and Ziegler-Graff, V. (2007) The Polerovirus F box protein P0 targets ARGONAUTE1 to suppress RNA silencing, Curr. Biol. *17*, 1615-1621.

Cieplak, W. Jr., Mead, D.J., Messer, R.J., and Grant, C.C. (1995). Site-directed mutagenic alteration of potential active-site residues of the A subunit of Escherichia coli heat-labile enterotoxin. Evidence for a catalytic role for glutamic acid 112. J. Biol. Chem. *270*, 30545-30550.

Clément, B., Pollmann, S., Weiler, E., Urbanczyk-Wochniak, E., and Otten, L. (2006). The Agrobacterium vitis T-6b oncoprotein induces auxin-independent cell expansion in tobacco. Plant J. *45*, 1017-1027.

Clough, S.J., and Bent, A.F. (1998). Floral dip: a simplified method for Agrocacterium-mediated transformation of Arabidopsis thaliana. Plant J. *16*: 735-743.

Deng, Q., and Barbieri, J.T. (2008). Molecular mechanisms of the cytotoxicity of ADP-ribosylating toxins. Annu. Rev. Microbiol. *62*, 271-288.

Doyle, J.D., Doyle, J.L., and Bailey, L.H. (1990). Isolation of plant DNA from fresh tissue. Focus *12*, 13-15

Fagard, M., Boutet, S., Morel, J.B., Bellini, C., Vaucheret, H. (2000). AGO1, QDE-2,

and RDE-1 are related proteins required for post-transcriptional gene silencing in plants, quelling in fungi, and RNA interference in animals. Proc Natl Acad Sci *97*, 11650-11654.

Fire, A., Xu, S.Q., Montgomery, M.K., Kostas, S.A., Driver, S.E., and Mello, C.C. (1998). Potent and specific genetic interference by double-stranded RNA in *Caenorhabditis elegans*. Nature *391*, 806-811.

Gális, I. I., Simek, P., Macas, J., Zahradnickova, H., Vlasak, J., Wabiko, H., Van Dongen, W., Van Onckelen, H. A., and Ondrej, M. (1999). The agrobacterium tumefaciens C58-6b gene confers resistance to N(6)-benzyladenine without modifying cytokinin metabolism in tobacco seedlings. Planta. *209*, 453-461.

Gális, I., Simek, P., Van Onckelen, H.A., Kakiuchi, Y., and Wabiko, H. (2002). Resistance of transgenic tobacco seedlings expressing the Agrobacterium tumefaciens C58-6b gene, to growth-inhibitory levels of cytokinin is associated with elevated IAA levels and activation of phenylpropanoid metabolism. Plant Cell Physiol. *43*, 939-950.

Garfinkel D.J., Simpson, R.B., Ream, L.W., White, F.F., Gordon, M.P., and Nester, E.W. (1981). Genetic analysis of crown gall: fine structure map of the T-DNA by site-directed mutagenesis. Cell *27*, 143–153.

Grémillon, L., Helfer, A., Clément, B., and Otten, L. (2004). New plant growth-modifying properties of the Agrobacterium T-6b oncogene revealed by the use of a dexamethasone-inducible promoter. Plant J. *37*, 218-228.

Guo, S., and Kemphues, K.J. (1995). *par-1*, a gene required for establishing polarity in *C.elegans* embryos, encodes a putative Ser/Thr kinase that is asymmetrically distributed. Cell *81*, 611-620.

Hammond, S.M., Bernstein, E., Beach, D., and Hannon, G.J. (2000). An RNA-directed nuclease mediates post-transcriptional gene silencing in Drosophila cells. Nature *404*, 293- 296.

Helfer, A., Clément, B., Michler, P., and Otten, L. (2003). The Agrobacterium oncogene AB-6b causes a graft-transmissible enation syndrome in tobacco. Plant Mol. Biol. *52*, 483-493.

Helfer, A., Pien, S., and Otten, L. (2002). Functional diversity and mutational analysis of Agrobacterium 6B oncoproteins. Mol. Genet. Genomics. *267*, 577-586.

Hooykaas, P.J.J., Den Dulk-Ras, H., and Schilperoort, R.A. (1988). The Agrobacterium tumefaciens T-DNA gene 6^b is an *onc* gene. Plant Mol. Biol. *11*,

791-794.

Huss, B., Tinland, B., Paulus, F., Walter, B., and Otten, L. (1990). Functional analysis of a complex oncogene arrangement in biotype III Agrobacterium tumefaciens strains. Plant Mol. Biol. *14*, 173-186.

Joos, H., Inzé, D., Caplan, A., Sormann, M., Van Montagu, M., and Schell, J. (1983). Genetic analysis of T-DNA transcripts in nopaline crown galls. Cell *32*, 1057–1067.

Kakiuchi, Y., Gális, I., Tamogami, S., and Wabiko, H. (2006). Reduction of polar auxin transport in tobacco by the tumorigenic Agrobacterium tumefaciens AK-6b gene. Planta. *223*, 237–247.

Kim, V.N. (2004). MicroRNA precursors in motion: exportin-5 mediates their nuclear export. Trends Cell Biol *14*, 156-159.

Kitakura, S., Fujita, T., Ueno, Y., Terakura, S., Wabiko, H., and Machida, Y. (2002). The protein encoded by oncogene 6b from Agrobacterium tumefaciens interacts with a nuclear protein of tobacco. Plant Cell *14*, 451–463.

Kitakura, S., Terakura, S., Yoshioka, Y., Machida, C., and Machida, Y. (2008) Interaction between Agrobacterium tumefaciens oncoprotein 6b and a tobacco nucleolar protein that is homologous to TNP1 encoded by a transposable element of Antirrhinum majus. J. Plant Res. *121*, 425-433.

Lakatos, L., Csorba, T., Pantaleo, V., Chapman, E.J, Carrington, J.C., Liu, Y.P., Dolja, V.V., Calvino, L.F., Lopez-Moya, J.J., and Burgyan, J. (2006). Small RNA binding is a common strategy to suppress RNA silencing by several viral suppressors. EMBO Journal *25*, 2768-2780.

Levesque, H., Delepelaire, P., Rouzé, P., Slightom, J., and Tepfer, D. (1988). Common evolutionary origin of the central portions of the Ri TL-DNA of Agrobacterium rhizogenes and the Ti T-DNAs of Agrobacterium tumefaciens. Plant Mol. Biol. *11*, 731–744.

Lobet, Y., Cluff, C.W., and Cieplak, W. Jr. (1991) Effect of site-directed mutagenic alterations on ADP-ribosyltransferase activity of the A subunit of *Escherichia coli* heat-labile enterotoxin. Infect. Immun. *59*, 2870-2879.

Mlotshwa, S., Voinnet, O., Mette, M.F., Matzke, M., Vaucheret, H., Ding, S.W., Pruss, G., and Vance, V.B. (2002). RNA silencing and the mobile silencing signal. Plant Cell *14*, S289-301.

Napoli, C., Lemieux,C. and Jorgensen,R. (1990). Introduction of a *chimeric chalcone synthase* gene into petunia results in reversible co-suppression of homologous genes in trans. The Plant Cell *2*, 279-289.

O'Neal, C.J., Amaya, E.I., Jobling, M.G., Holmes, R.K., and Hol, W.G. (2004). Crystal structures of an intrinsically active cholera toxin mutant yield insight into the toxin activation mechanism. Biochemistry *43*, 3772-3782.

Parker, J.S., Roe, S.M., and Barford, D. (2005). Structural insights into mRNA recognition from a PIWI domain-siRNA guide complex. Nature *434*, 663-666.

Paulus, F., Huss, B., Tinland, B., Herrmann, A., Canaday, J., and Otten, L. (1991). Role of T-region borders in Agrobacterium host range. Mol. Plant-Microb. Interact. *4*, 163-172.

Romano, N., Macino, G. (1992). Quelling: transient inactivation of gene expression in *Neurospora crassa* by transformation with homologous sequences. Mol Microbiol *6*, 3343- 3353.

Sambrook, J., Fritsch, E.F., and Maniatis, T. (1989). Molecular Cloning: A laboratory manual, 2nd ed. Cold Spring Harbor Laboratory Press.

Schnettler, E., Hemmes, H., Goldbach, R. and Prinst, M. (2008). The NS3 protein of *rice hoja blanca virus* suppresses RNA silencing in mammalian cells. J Gen Virol 89,3:36-340.

Sontheimer, E.J. (2005). Assembly and function of RNA silencing complexes. Nature Reviews Molecular Cell Biology 6, 127-138.

Spanier, K., Schell, J., and Schreier, P.H. (1989). A functional analysis of T-DNA gene 6b: the fine tuning of cytokinins effects on shoot development. Mol. Gen. Genet. *219*, 209-216.

Spena, A., Schmülling, T., Koncz, C., and Schell, J.S. (1987). Independent and synergistic activity of rol A, B and C loci in stimulating abnormal growth in plants. EMBO J *6*, 3891–3899.

Stieqer, P.A., Meyer, A.D., Kathmann, P., Fründt, C., Niederhauser, I., Barone, M., and Kuhlemeier, C. (2004). The orf13 T-DNA gene of Agrobacterium rhizogenes confers meristematic competence to differentiated cells. Plant Physiol. *135*, 1798–1808.

Terakura, S., Kitakura, S., Ishikawa, M., Ueno, Y., Fujita, T., Machida, C., Wabiko, H., and Machida, Y. (2006). Oncogene 6b from Agrobacterium tumefaciens induces

abaxial cell division at late stages of leaf development and modifies vascular development in petioles. Plant Cell Physiol. *47*, 664–672.

Terakura, S., Ueno, Y., Taqami, H., Kitakura, S., Machida, C., Wabiko, H., Aiba, H., Otten, L., Tsukaqoshi, H., Nakamura, K., and Machida, Y. (2007). An oncoprotein from the plant pathogen agrobacterium has histone chaperone-like activity. Plant Cell. *19*, 2855-2865.

Tinland, B., Huss, B., Paulus, F., Bonnard., G., and Otten, L. (1989). Agrobacterium tumefaciens 6b genes are strain-specific and affect the activity of auxin as well as cytokinin genes. Mol. Gen. Genet. *219*, 217-224.

Tinland, B., Rohfritsch, O., Michler, P., and Otten, L. (1990). Agrobacterium tumefaciens T-DNA gene 6b stimulates rol-induced root formation, permits growth at high auxin concentrations and increases root size. Mol. Gen. Genet. *223*, 1-10.

Tinland, B., Fournier, P., Heckel, T., and Otten, L. (1992). Expression of a chimaeric heat-shock-inducible Agrobacterium 6b oncogene in Nicotiana rustica. Plant Mol. Biol. *18*, 921-930.

Van den Akker, F., Merritt, E.A., Pizza, M., Domenighini, M., Rappuoli, R., and Hol, W.G. (1995). The Arg7Lys mutant of heat-labile enterotoxin exhibits great flexibility of active site loop 47-56 of the A subunit. Biochemistry *34*, 10996-11004.

Wabiko, H., and Minemura, M. (1996). Exogenous phytohormone-independent growth and regeneration of tobacco plants transgenic for the 6b gene of Agrobacterium tumefaciens AKE10. Plant Physiol. *112*, 939–951.

Willmitzer L., Dhaese P, Schreier PH, Schmalenbach W, Van Montagu M, Schell J (1983) Size, location and polarity of T-DNA-encoded transcripts in nopaline crown gall tumors: common transcripts in octopine and nopaline tumors. Cell *32*, 1045-1056.

Yates, S.P., Taylor, P.J., Joergensen, R., Ferrraris, D., Zhang, J., Andersen, G.R., and Merrill, A.R. (2005). Structure-function analysis of water-soluble inhibitors of the catalytic domain of exotoxin A from Pseudomonas aeruginosa. Biochem. J. *385*, 667-675.

Yang, J. and Yuan, Y.A. (2009) A structural perspective of the protein-RNA interactions involved in virus-induced RNA silencing and its suppression. Biochim. Biophys. Acta. Jun. 6.

Yi, R., Qin, Y., Macara, I.G., and Cullen, B.R. (2003). Exportin-5 mediates the nuclear export of pre-microRNAs and short hairpin RNAs. Genes Dev *17*, 3011-3016.

Zhang, X., Henriques, R., Lin, S.S., Niu, Q.W., and Chua, N.H. (2006). Agrobacterium-mediated transformation of Arabidopsis thaliana using the floral dip method. Nat. Protoc. *1*, 641-646.

Zhang, X., Yuan, Y.R., Pei, Y., Lin, S.S., Tuschl, T., Patel, D.J. and Chua, N.H. (2006). Cucumber mosaic virus-encoded 2b suppressor inhibits Arabidopsis Argonaute1 cleavage activity to counter plant defense. Genes Dev. *20*, 3255–3268.

Appendix

Table A1. Preparation of stock solution of Murashige and Skoog (MS) medium

Constituent	Concentration in MS medium (mg/l)	Concentration in the stock solution (mg/l)
Macronutrients (10X)		
NH_4NO_3	1650	16500
KNO_3	1900	19000
$MgSO_4•7H_2O$	370	3700
$CaCl_2•2H_2O$	440	4400
KH_2PO_4	170	1700
Micronutrients (100X)		
H_3BO_3	6.2	620
$MnSO_4•4H_2O$	22.3	2230
$ZnSO_4•7H_2O$	8.6	860
KI	0.83	830
$Na_2MoO_4•2H_2O$	0.25	25
$CuSO_4•5H_2O$	0.025	2.5
$CoCl_2•6H_2O$	0.025	2.5
Iron source		
Fe•EDTA-Na salt	40	Added fresh
Vitamins		
Nicotinic acid	0.5	50mg/100ml
Thiamine HCl	0.1	10mg/100ml
Pyridoxine HCl	0.5	50mg/100ml
Others		
Myo-inositol	100	Added fresh
Glycine	2	50mg/100ml
Sucrose	30,000	Added fresh
Agar	8000	Added fresh
pH5.8		

Table A2. Plasmids Used in this study

Plasmid	Relevant Characteristics
Vectors for protein synthesis in *Escherichia Coli*	
pET-Ak6b	Derivative of pET-28b containing His-AK6b DNA
pGEX-Ak6b	Derivative of pGEX -6p-1 containing GST-AK6b DNA
pGEX-200	Derivative of pGEX -6p-1 containing GST-AK6b (Δ200-208aa) DNA
pETAB6b	Derivative of pET-28b containing His-AB6b DNA
pGEX-AB6b	Derivative of pGEX -6p-1 containing GST-AB6b DNA
pET-H3	Derivative of pET-28b-SUMO containing His-SUMO-H3 DNA
pET-SE	Derivative of pET-28b containing His-SE core DNA
pGEX-Mid	Derivative of pGEX -6p-1 containing GST-SE-Mid DNA
pGEX-NT	Derivative of pGEX -6p-1 containing GST-SE-NT DNA
pMAL-Ak6b	Derivative of pMAL –c2X-1 containing MBP-AK6b DNA
pMAL-40	Derivative of pMAL –c2X-1 containing MBP-AK6b (Δ40-55aa) DNA
pMAL-164	Derivative of pMAL –c2X-1 containing MBP-AK6b (Δ164-184aa) DNA
pMAL-PolyQ	Derivative of pMAL –c2X-1 containing MBP-AGO1-PolyQ DNA
pMAL-NT	Derivative of pMAL –c2X-1 containing MBP- AGO1-NT DNA
pMAL-PAZ	Derivative of pMAL –c2X-1 containing MBP- AGO1-PAZ DNA
pMAL-MID	Derivative of pMAL –c2X-1 containing MBP- AGO1-MID DNA
pMAL-PIWI1	Derivative of pMAL –c2X-1 containing MBP- AGO1-PIWI1 DNA
pMAL-PIWI2	Derivative of pMAL –c2X-1 containing MBP- AGO1-PIWI2 DNA
Binary vectors for transformation of Arabidopsis	
p121-Ak6b	Derivative of pBI121 containing 35S::AK6b DNA
p121-40	Derivative of pBI121 containing 35S::AK6b (Δ40-55aa) DNA
p121-116	Derivative of pBI121 containing 35S::AK6b (Δ116-119aa) DNA
p121-121	Derivative of pBI121 containing 35S::AK6b (Y121A) DNA
p121-123	Derivative of pBI121 containing 35S::AK6b (Δ121-123aa) DNA
p121-66	Derivative of pBI121 containing 35S::AK6b (Y66A) DNA
p121-93	Derivative of pBI121 containing 35S::AK6b (T93A) DNA
p121-146	Derivative of pBI121 containing 35S::AK6b (D146A) DNA
Vectors for transformation of onion epidermal cells	
pBA002-YFP	Derivative of pBA002 containing 35S::YFP DNA
pBA002- CFP	Derivative of pBA002 containing 35S::CFP DNA
pBA002-AK6b-YFP	Derivative of pBA002 containing 35S::AK6b-YFP DNA
pBA002-Ago1-CFP	Derivative of pBA002 containing 35S::Ago1-CFP DNA
pBA002-SE-CFP	Derivative of pBA002 containing 35S::SE-CFP DNA
See text for details.	

Table A3: Primers used for the construction of point mutation or depletion within the AK6b coding sequence. Alanine substitutions residues were shown in bold red.

Region specific primer	Forward	Reserve
Δ40-55aa	CCACCCTGTCACAATTCGTAgcgCTCCTTTCAGACCAGAGGC	GCCTCTGGTCTGAAAGGAGcgcTACGAATTGTGACAGGGTGG
Δ116-119aa	CAACAGAGTTGCGGTCAAgcgAATTACCACCACGGTCC	CGGACCGTGGTGGTAATTcgcTTGACCGCAACTCTGTTG
Δ121-123aa	GTCAAGGAGGCTTCGTTAATgcggcggcgGGTCCGAGTACAAACAGCTT	AAGCTGTTTGTACTCGGACCcgccgccgcATTAACGAAGCCTCCTTGAC
Δ164-184aa	GCCAGGCTAGGTAATTATGTTgcgACGAGAGAGTTCCAATTATCC	GGATAATTGGAACTCTCTCGTcgcAACATAATTACCTAGCCTGGC
Δ200-208aa	GTAGCTctcgagTTACTAGACAATGGGATAATGAATGAGAT	GTAGCTaagcttTTACTAGACAATGGGATAATGAATGAGAT
T93A	GCCTTCGGGACAGTAGCTgcgGCAATGCCCCCATGG	CCATGGGGGCATTGCcgcAGCTACTGTCCCGAAGGC
Y121A	GTCAAGGAGGCTTCGTTAATgcgCACCACGGTCCGAGTACA	TGTACTCGGACCGTGGTGcgcATTAACGAAGCCTCCTTGAC
D146A	TTGTTCATACGGATCAGGACTgcgGTAATCCGCGGTCAAGGT	ACCTTGACCGCGGATTACcgcAGTCCTGATCCGTATGAACAA

Novagen

pET-28a-c(+) Vectors

TB074 12/98

	Cat. No.
pET-28a DNA	69864-3
pET-28b DNA	69865-3
pET-28c DNA	69866-3

The pET-28a-c(+) vectors carry an N-terminal His• Tag®/thrombin/T7• Tag® configuration plus an optional C-terminal His• Tag sequence. Unique sites are shown on the circle map. Note that the sequence is numbered by the pBR322 convention, so the T7 expression region is reversed on the circular map. The cloning/expression region of the coding strand transcribed by T7 RNA polymerase is shown below. The f1 origin is oriented so that infection with helper phage will produce virions containing single-stranded DNA that corresponds to the coding strand. Therefore, single-stranded sequencing should be performed using the T7 terminator primer (Cat. No. 69337-3).

pET-28a(+) sequence landmarks	
T7 promoter	370-386
T7 transcription start	369
His• Tag coding sequence	270-287
T7• Tag coding sequence	207-239
Multiple cloning sites (*Bam*H I - *Xho* I)	158-203
His• Tag coding sequence	140-157
T7 terminator	26-72
lacI coding sequence	773-1852
pBR322 origin	3286
Kan coding sequence	3995-4807
f1 origin	4903-5358

The maps for pET-28b(+) and pET-28c(+) are the same as pET-28a(+) (shown) with the following exceptions: pET-28b(+) is a 5368bp plasmid; subtract 1bp from each site beyond *Bam*H I at 198. pET-28c(+) is a 5367bp plasmid; subtract 2bp from each site beyond *Bam*H I at 198.

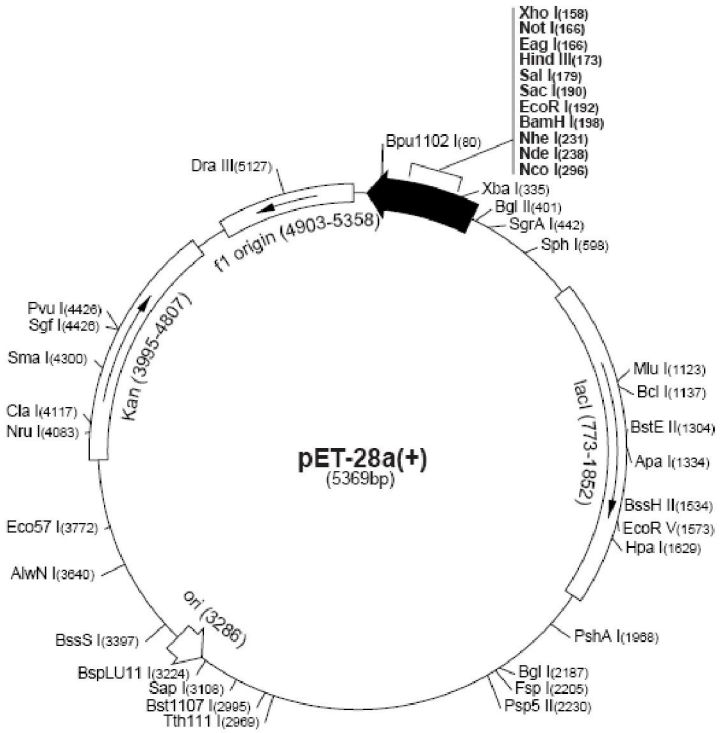

Fig. 1A pET-28b vector with his tag was used in plasmid construction for protein expression in *E.coli*.

pGEX Vectors*(GST Gene fusion)

All of the GST gene fusion vectors offer:

- *A tac promoter for chemically inducible, high-level expression.*

pGEX-1λT (27-4805-01)
Thrombin
Leu Val Pro Arg↓Gly Ser Pro Glu Phe Ile Val Thr Asp
CTG GTT CCG CGT GGA TCC CCG GAA TTC ATC GTG ACT GAC TGA CGA
BamH I EcoR I Stop codons

pGEX-2T (27-4801-01)
Thrombin
Leu Val Pro Arg↓Gly Ser Pro Gly Ile His Arg Asp
CTG GTT CCG CGT GGA TCC CCG GGA ATT CAT CGT GAC TGA CTG ACG
BamH I Sma I EcoR I Stop codons

pGEX-2TK (27-4587-01)
Thrombin Kinase
Leu Val Pro Arg↓Gly Ser Arg Arg Ala Ser Val
CTG GTT CCG CGT GGA TCT CGT CGT GCA TCT GTT GGA TCC CCG GGA ATT CAT CGT GAC TGA
BamH I Sma I EcoR I Stop codons

pGEX-4T-1 (27-4580-01)
Thrombin
Leu Val Pro Arg↓Gly Ser Pro Glu Phe Pro Gly Arg Leu Glu Arg Pro His Arg Asp
CTG GTT CCG CGT GGA TCC CCG GAA TTC CCG GGT CGA CTC GAG CGG CCG CAT CGT GAC TGA
BamH I EcoR I Sma I Sal I Xho I Not I Stop codons

pGEX-4T-2 (27-4581-01)
Thrombin
Leu Val Pro Arg↓Gly Ser Pro Gly Ile Pro Gly Ser Thr Arg Ala Ala Ala Ser
CTG GTT CCG CGT GGA TCC CCA GGA ATT CCC GGG TCG ACT CGA GCG GCC GCA TCG TGA
BamH I EcoR I Sma I Sal I Xho I Not I Stop codon

pGEX-4T-3 (27-4583-01)
Thrombin
Leu Val Pro Arg↓Gly Ser Pro Asn Ser Arg Val Asp Ser Ser Gly Arg Ile Val Thr Asp
CTG GTT CCG CGT GGA TCC CCG AAT TCC CGG GTC GAC TCG AGC GGC CGC ATC GTG ACT GAC TGA
BamH I EcoR I Sma I Sal I Xho I Not I Stop codons

pGEX-3X (27-4803-01)
Factor Xa
Ile Glu Gly Arg↓Gly Ile Pro Gly Asn Ser Ser
ATC GAA GGT CGT GGG ATC CCC GGG AAT TCA TCG TGA CTG ACT GAC
BamH I Sma I EcoR I Stop codons

pGEX-5X-1 (27-4584-01)
Factor Xa
Ile Glu Gly Arg↓Gly Ile Pro Glu Phe Pro Gly Arg Leu Glu Arg Pro His Arg Asp
ATC GAA GGT CGT GGG ATC CCC GAA TTC CCG GGT CGA CTC GAG CGG CCG CAT CGT GAC TGA
BamH I EcoR I Sma I Sal I Xho I Not I Stop codons

pGEX-5X-2 (27-4585-01)
Factor Xa
Ile Glu Gly Arg↓Gly Ile Pro Gly Ile Pro Gly Ser Thr Arg Ala Ala Ala Ser
ATC GAA GGT CGT GGG ATC CCC GGA ATT CCC GGG TCG ACT CGA GCG GCC GCA TCG TGA
BamH I EcoR I Sma I Sal I Xho I Not I Stop codon

pGEX-5X-3 (27-4586-01)
Factor Xa
Ile Glu Gly Arg↓Gly Ile Pro Arg Asn Ser Arg Val Asp Ser Ser Gly Arg Ile Val Thr Asp
ATC GAA GGT CGT GGG ATC CCC AGG AAT TCC CGG GTC GAC TCG AGC GGC CGC ATC GTG ACT GAC TGA
BamH I EcoR I Sma I Sal I Xho I Not I Stop codons

pGEX-6P-1 (27-4597-01)
PreScission™ Protease
Leu Glu Val Leu Phe Gln↓Gly Pro Leu Gly Ser Pro Glu Phe Pro Gly Arg Leu Glu Arg Pro His
CTG GAA GTT CTG TTC CAG GGG CCC CTG GGA TCC CCG GAA TTC CCG GGT CGA CTC GAG CGG CCG CAT
BamH I EcoR I Sma I Sal I Xho I Not I

pGEX-6P-2 (27-4598-01)
PreScission™ Protease
Leu Glu Val Leu Phe Gln↓Gly Pro Leu Gly Ser Pro Gly Ile Pro Gly Ser Thr Arg Ala Ala Ala Ser
CTG GAA GTT CTG TTC CAG GGG CCC CTG GGA TCC CCA GGA ATT CCC GGG TCG ACT CGA GCG GCC GCA TCG
BamH I EcoR I Sma I Sal I Xho I Not I

pGEX-6P-3 (27-4599-01)
PreScission™ Protease
Leu Glu Val Leu Phe Gln↓Gly Pro Leu Gly Ser Pro Asn Ser Arg Val Asp Ser Ser Gly Arg
CTG GAA GTT CTG TTC CAG GGG CCC CTG GGA TCC CCG AAT TCC CGG GTC GAC TCG AGC GGC CGC
BamH I EcoR I Sma I Sal I Xho I Not I

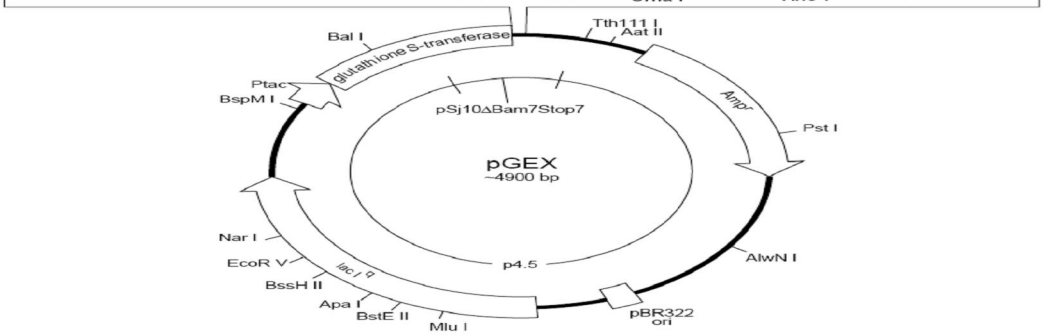

Map of the glutathione S-transferase fusion vectors showing the reading frames and main features. Even though stop codons in all three frames are not depicted in this map, all thirteen vectors have stop codons in all three frames downstream from the multiple cloning site.

Fig. 2A pGEX-6P-1 vector with GST tag was used in plasmid construction for protein expression in *E.coli*.

System Components & Companion Products

Vectors

The pMAL-c2 series of vectors have an exact deletion of the *malE* signal sequence, resulting in cytoplasmic expression of the fusion protein. The pMAL-p2 series of vectors contain the normal *malE* signal sequence, which directs the fusion protein through the cytoplasmic membrane. All of the vectors include a sequence coding for the recognition site of a specific protease (Factor Xa [X], Enterokinase [E] or Genenase™ I [G]) which allows the protein of interest to be cleaved from MBP after purification.

pMAL™ Vectors

pMAL-c2X
#N8076S 10 µg .....$75 (USA)

pMAL-p2X
#N8077S 10 µg .....$75 (USA)

Note: pMAL-c2X and pMAL-p2X are supplied with the pMAL Protein Fus and Purification System (NEB #E8000S).

pMAL-c2E *(not supplied with the system)*
#N8066S 10 µg .....$75 (USA)

pMAL-p2E *(not supplied with the system)*
#N8067S 10 µg .....$75 (USA)

pMAL-c2G *(not supplied with the system)*
#N8068S 10 µg .....$75 (USA)

pMAL-p2G *(not supplied with the system)*
#N8069S 10 µg .....$75 (USA)

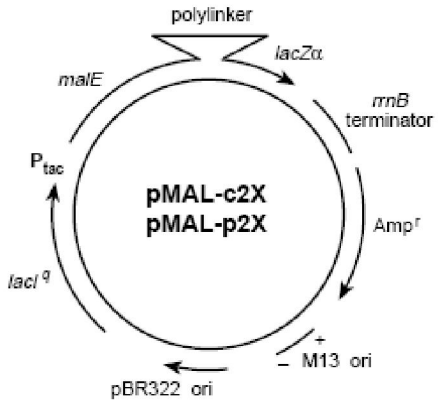

pMAL™-c2X, -p2X polylinker:

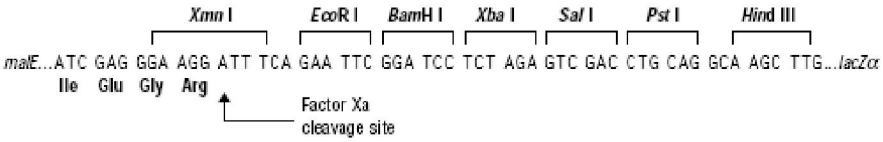

pMAL-c2E, pMAL-p2E Polylinker

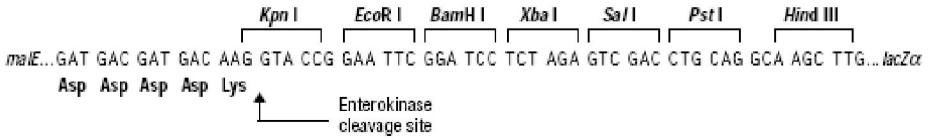

pMAL-c2G, pMAL-p2G Polylinker

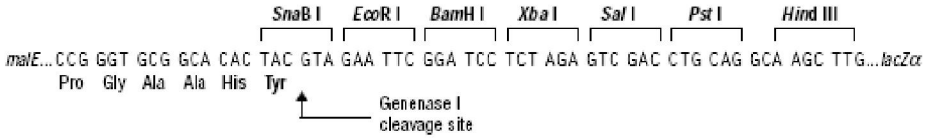

Fig. 3A pMAL-c2X vector with MBP tag was used in plasmid construction for protein expression in *E.coli*.

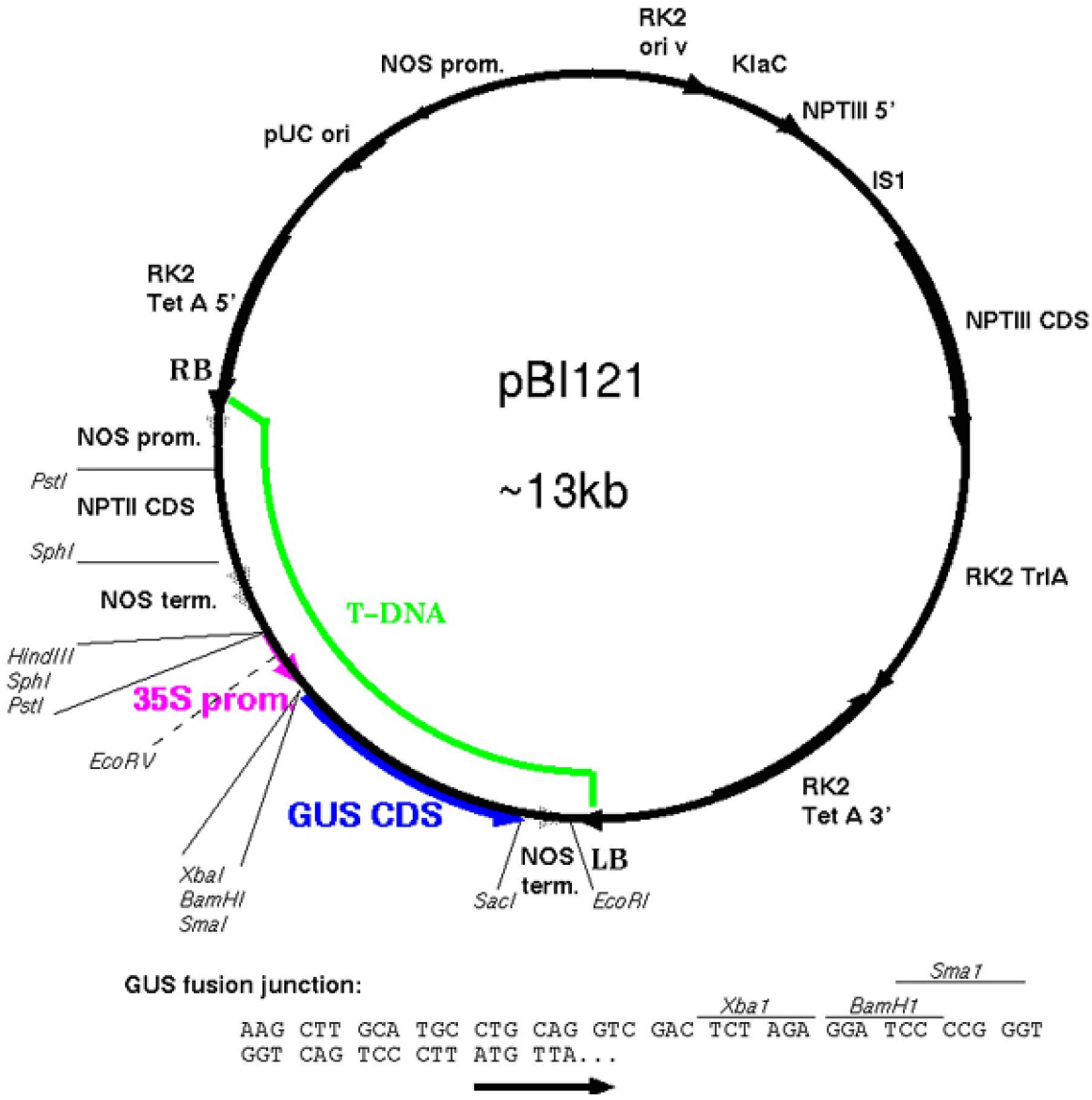

pBI121 (Clontech Inc.) - an *E.coli/A.tumefaciens* shuttle vector, designed to excise T-DNA insert using vir functions in *A.tumefaciens*, using vir functions supplied *in-trans* by a disarmed Ti plasmid.

T-DNA：

- **RB, LB** - nopaline T-DNA right borders
- **NOS-NPTII-NOS** - Chimeric gene for kanamycin resistance. Neomycin phosphotransferase gene under the control of nopaline synthase promoter and terminator, which can be used to assay for presence of construct in transformant plant.
- **35S/GUS CDS** - *E. coli* β-glucuronidase reporter gene (GUS) protein coding sequence (CDS) controlled by the constitutive 35S promoter from CaMV.

Fig. 4A pBA121 vector with CaMV 35S promoter was used in plasmid construction for transformation of *Arabidopsis*.

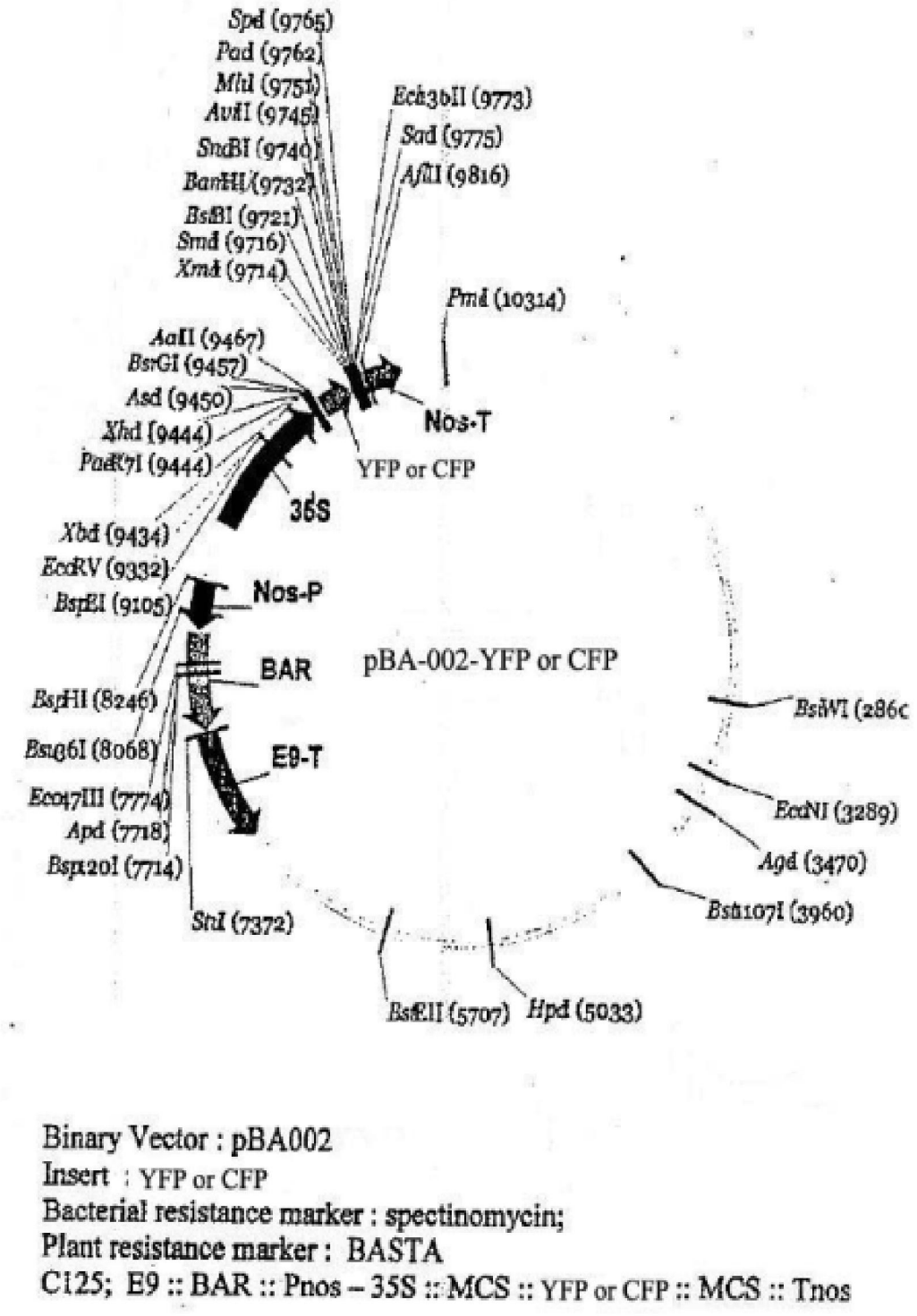

Fig. 5A pBA002 vector with CaMV 35S promoter and YFP or CFP protein was used in plasmid construction for particle bombardment into onion epidermal cells.

Publications

1. **Mei-Mei Wang**1,2, Takashi Soyano3, Jun-Yi Yang3, Choonkyun Jungv3, Nam-Hai Chua3 and Y. Adam Yuan1,2,* Structural insights into plant cell proliferation disturbance by Agrobacterium protein 6b. Plant Journal (under review).

2. Wen-Ying Liu1, Mei-Mei Wang1, Ji Huang, Hai-Juan Tang, Hong-Xia Lan and Hong-Sheng Zhang. The *OsDHODH1* Gene is Involved in Salt and Drought Tolerance in Rice. Journal of Integrative Plant Biology. 2009, 51(9): 825-833.

3. Ji Huang, **Mei-Mei Wang**, Yan Jiang, Yong-Mei Bao, Xi Huang, Hui Sun, Dong-Qing Xu, Hong-Xia Lan, Hong-Sheng Zhang. Expression analysis of rice A20/AN1-type zinc finger genes and characterization of ZFP177 that contributes to temperature stress tolerance. Gene 420 (2008) 135-144.

4. Ji Huang, **Mei-Mei Wang**, Yan Jiang, Qi-Hong Wang, Xi Huang, Hong-Sheng Zhang. Stress repressive expression of rice SRZ1 and characterization of plant SRZ gene family. Plant Science 174 (2008) 227-235.

5. Ji Huang[1], Xia Yang[1], **Mei-Mei Wang**, Hai-Juan Tang, Lin-Yun Ding, Yin Shen, Hong-sheng Zhang. A novel rice C2H2-type zinc finger protein lacking DLN-box/EAR-motif plays a role in salt tolerance. Biochimica et Biophysica Acta, 2007.

6. Qiu SP, Huang J, Pan LJ, **Wang MM**, Zhang HS. Salt induces expression of RH3.2A, encoding an H3.2-type histone H3 protein in rice (*Oryza sativa L.*), Acta Genetica Sinica, 2006, 33(9): 833-840.